Fluvio-deltaic record of increased sediment transport during the Middle Eocene Climatic Optimum (MECO), Southern Pyrenees, Spain

Sabí Peris Cabré[1, 2], Luis Valero[1], Jorge E. Spangenberg[3], Andreu Vinyoles[4], Jean Verité[1, 5], Thierry Adatte[6], Maxime Tremblin[1], Stephen Watkins[1], Nikhil Sharma[1], Miguel Garcés[4], Cai ~~Puigdefàbregas[1]~~Puigdefàbregas[2], Sébastien ~~Castelltort[2]~~Castelltort[1]

[1]Département des Sciences de la Terre, Université de Genève, Genève, 1205, Switzerland
[2]Departament de Geologia, Universitat Autònoma de Barcelona, Cerdanyola del Vallès, 08193, Spain
[3]Institute of Earth Surface Dynamics (IDYST), University of Lausanne, Géopolis, Lausanne, 1015, Switzerland
[4]Departament de Dinàmica de la Terra i l'Oceà, Facultat de Ciències de la Terra, Barcelona, 08028, Spain
[5]Départment des Geosciences, Université de Rennes, Rennes, UMR 6118, France
[6]Institute of Earth Sciences (ISTE), University of Lausanne, Géopolis, Lausanne, 1015, Switzerland

Correspondence to: Sabí Peris Cabré (sabi.peris@uab.cat)

Abstract. The early Cenozoic marine sedimentary record is punctuated by several brief episodes (< 200 kyr) of abrupt global warming, called hyperthermals, that have disturbed ocean life and water physicochemistry. Moreover, recent studies of fluvial-deltaic systems, for instance at the Palaeocene-Eocene Thermal Maximum, revealed that these hyperthermals also impacted the hydrologic cycle, triggering an increase in erosion and sediment transport at the Earth's surface. Contrary to the early Cenozoic hyperthermals, the Middle Eocene Climatic Optimum (MECO), lasting from 40.5 to 40.0 Ma, constitutes an event of gradual warming that left a highly variable carbon isotope~~ic~~ signature and for which little data exist about its impact on Earth surface systems. In the South-Pyrenean Foreland Basin (SPFB), an episode of prominent deltaic progradation (Belsué-Atarés and Escanilla formations) in the middle Bartonian has been usually associated with increased Pyrenean tectonic activity, ~~but~~but recent ~~recent~~ magnetostratigraphic data suggest a possible coincidence between the progradation and the MECO warming period. To test this hypothesis, we measured the stable isotop~~ice~~e composition of carbonates ($\delta^{13}C_{carb}$ and $\delta^{18}O_{carb}$) and organic matter (-$\delta^{13}C_{org}$) of 257 samples in two sections of SPFB fluvial-deltaic successions covering the different phases of the MECO and already dated with magnetostratigraphy. We find a negative shift in $\delta^{18}O_{carb}$ and an unclear signal in $\delta^{13}C_{carb}$ around the transition from magnetic Chron C18r to Chron C17r (middle Bartonian). These results allow, by correlation with reference sections in the Atlantic and Tethys, to identify the MECO and document its coincident relationship with the Belsué-Atarès fluvial-deltaic progradation. Despite its long duration and a more gradual temperature rise, the MECO in the South Pyrenean Foreland Basin may have led, like lower Cenozoic hyperthermals, to an increase in erosion and sediment transport that is manifested in the sedimentary record. The new data support the hypothesis of a more important hydrological response to the MECO than previously thought in ~~mid~~ mid-latitude environments, including those around the Tethys.

1 Introduction

The Middle Eocene Climatic Optimum (MECO) is a global warming event that occurred during the Bartonian (ca. 40.5 – 40.0 Ma~~), and which)~~ and briefly reversed the longer-term cooling trend of the middle to upper Eocene (Fig. 1; Arimoto *et al.*, 2020; Bijl et al., 2010; Bohaty and Zachos, 2003; Bohaty *et al.*, 2009; Bosboom *et al.*, 2014; Galazzo *et al.*, 2014; Henehan *et al.*, 2020; Edgar *et al.*, 2010, 2020; ~~Giorgini~~Giorgioni *et al.*, 2019; Jovane *et al.*, 2007; Mulch *et al.*, 2015; Sluijs *et al.*, 2013; Sppoforth *et al.*, 2010; Pälike *et al.*, 2012; van der Boon *et al.*, 2020). Marine bulk and benthic oxygen isotope compositions (δ^{18}O values) ~~both~~ show a negative excursion of -1.5 ‰ over the event, which was interpreted as a gradual global warming of 3 to 6ºC (Bohaty et al., 2009). ~~. The evolution of carbon isotope composition δ^{13}C, in~~ In contrast, the evolution of carbon isotope composition (δ^{13}C values), ~~and~~ unlike earlier hyperthermals of the Cenozoic (e.g., Palaeocene-Eocene Thermal Maximum PETM, Eocene Thermal Maximum ETM 2 among others), differs from site to site, showing opposite patterns between hemispheres ~~-~~and displaying ~~displaying~~ a carbon isotope excursion (CIE) in some but not all marine records (Bohaty *et al.*, 2009; Henehan *et al.*, 2020; Westerhold and Röhl, 2013). This CIE suggests a ~~raise~~ rise in atmospheric partial pressure of carbon dioxide (pCO_2) during the warming peak (Henehan *et al.*, 2020; Bijl *et al.*, 2010), and numerous potential CO_2 sources have been proposed. Among them, a prolonged pulse of metamorphic decarbonization possibly linked with the Himalayan collision at that time (Bijl *et al.*, 2010; Bohaty *et al.*, 2009, Bouilhol *et al.*, 2013, Sternai *et al.*, 2020), an increase of volcanism (van der Boon *et al.* 2020), or lower continental weatherability (van der Ploeg *et al.* 2018). However, the pCO_2 record remains ambiguous and difficult to link in a straightforward way to a rapid injection of exogenous carbon during the MECO (e.g., Henehan *et al.*, 2020). In addition, regardless of the CO_2 sources involved, the MECO coincides with a very long (2.~~4~~ 4 Myr) ~~very long-term~~ eccentricity cycle, ~~(2.4 My) minima (Westerhold & Röhl, 2013), which~~ suggest~~s~~ing a possible orbital trigger (Westerhold ~~&~~ and Röhl, 2013~~, Henehan et al. 2020~~). Therefore, considering the unresolved MECO driving mechanism(s), and how the Earth system responded to this carbon cycle perturbation, the MECO poses a significant challenge to understanding carbon cycle variations on timescales of several hundreds of thousands of years (Sluijs *et al.*, 2013; Henehan *et al.*, 2020; Sternai *et al.*, 2020). Addressing this challenge requires extensive documentation of the MECO in a range of environments and geodynamic contexts, as well as documentation of its effect on ~~earth~~Earth surface dynamics.

~~is currently considered as a key problem in paleoclimate research, holding keys about our understanding of the global carbon cycle in the larger context of the solid and fluid Earth interactions (Sluijs et al., 2013; Henehan et al., 2020; Sternai et al., 2020).~~

Current data converge towards the view that, during the MECO, surface and deep oceanic waters ~~suffered~~ experienced a gradual and uniform warming between 3 to 6°C for all latitudes (Arimoto *et al.*, 2020; Bijl *et al.*, 2010; Bohaty *et al.*, 2009; Rivero-Cuesta *et al.*, 2019). Moreover, deep-sea carbonates were affected either by ~~very~~ significantly reduced carbonate accumulation rates or even by dissolution, suggesting broad acidification of sea-bottom waters, involving an estimated *ca* ~~1~~ 1 km shoaling of the carbonate compensation depth (CCD; Henehan *et al.*, 2020; Cornaggia *et al.* 2020; Pälike *et al.* 2012; Arimoto *et al.*, 2020). However, while the temperature increase in the oceans has been inferred in multiple sites, the MECO

Con formato: Fuente: Cursiva
Con formato: Fuente: Cursiva
Con formato: Fuente: Cursiva
Con formato: Fuente: Cursiva
Con formato ...
Con formato: Fuente: Cursiva
Con formato ...
Con formato: Fuente: Cursiva
Con formato: Fuente: Cursiva
Con formato ...
Con formato: Fuente: Cursiva
Con formato: Fuente: Cursiva
Con formato: Subíndice
Con formato ...
Con formato: Fuente: Cursiva
Con formato: Fuente: Cursiva
Con formato ...
Con formato ...
Con formato ...
Con formato: Color de fuente: Rojo
Con formato ...
Con formato ...
Con formato ...
Con formato ...
Con formato ...
Con formato: Fuente: Cursiva
Con formato: Fuente: Cursiva
Con formato: Fuente: Cursiva
Con formato: Fuente: Cursiva

environmental perturbation affected differently the fauna communities (Arimoto *et al*., 2020). In some locations, the warmer conditions reduced nutrient availability, decreasing the benthic productivity (Arimoto *et al*., 2020; Bijl *et al*., 2010, Galazzo *et al*., 2014; Moebius *et al*., 2015). ~~Whereas~~In contrast, the Southern Ocean (Moebius *et al*., 2014) or the Neo-Tethys Ocean (Galazzo *et al*., 2013) record increased productivity during the MECO.

~~Finally, this significant environmental perturbation seems to have caused widespread ocean stratification and eutrophic conditions, starving the benthic foraminiferal communities during the climax of MECO warmth (Galazzo et al., 2014; Arimoto et al. 2020; Cramwinckel et al. 2019).~~

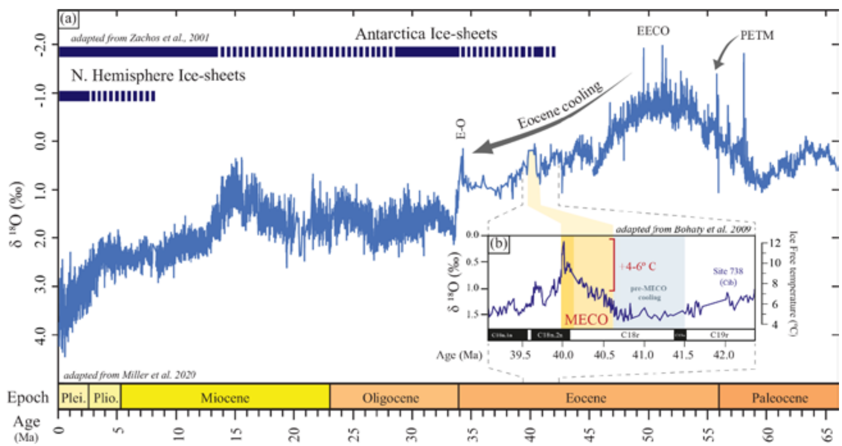

Figure 1: (a) Cenozoic δ^{18}O values compilation from the Pacific Ocean, compiled in Miller et al. (2020). The continuous blue bar represents permanent ice sheet presence, and the discontinuous blue bar represents ephemeral ice sheet, modified from Zachos *et al.* (2001). Main climate events, EECO: Early Eocene Climatic Optimum; PETM: Palaeocene Eocene Thermal Maximum, MECO: Middle Eocene Climatic Optimum, E-O: Eocene Oligocene transition. (b) Carbonate δ^{18}O values ~~from of~~ site 702~~, by~~ from Bohaty *et al*~~., ~~ (2009). General climatic context of the Middle Eocene Climatic Optimum. The MECO "event", in yellow from ca 40.5 ~~5 Ma~~ to ~~40~~ 40.0 Ma in the inset, is considered the last ~~"~~hyperthermal~~"~~ of the Eocene, immediately preceding the shift to genuine Antarctic glaciation and the ice-house world of the Oligocene.

In contrast to the oceanic realm, the expression of the MECO in non-marine records remains scarce and variable. Mulch *et al.* (2015) suggested a boost of precipitation in the North American plateau derived from low δ^{18}O values, while Bosboom *et al.* (2014) documented a shift towards arid conditions in the Tarim Basin with a reduction in fern palynomorphs. Such drying trend in central Asia is opposite to the Neo-Tethys ~~ocean~~ Ocean dynamic, where a greater burial of organic matter (OM) immediately following the MECO may have been caused by increased nutrients runoff due to an enhanced hydrological cycle during the warm period (Galazzo *et al*., 2014; Giorgioni *et al*., 2019; Spofforth *et al*., 2010). These studies raise the question of the response of weathering, erosion, and sediment transport in terrestrial systems to global warming, as it has also been posed ~~also~~ for other hyperthermals recently (e.g., Chen *et al*., 2018; Foreman *et al*., 2012, 2017; Honegger *et al*., 2020). This issue highlights the need for further documentation of the clastic sedimentary successions that temporally cover single and long-term climate crises (~~i.e~~i.e.,~~.~~ Early Eocene Climatic Optimum, Palaeocene Eocene Thermal Maximum, etc.; Fig. 1).

In this work, we aim to understand the effects of the MECO on surface systems by exploring the interface between ocean and continent. The shallow marine settings, very sensitive to sea level changes and sediment supply, potentially ~~provides~~ provide a unique perspective of the hydrological response to climate change in the continental domain~~, as well as~~ and geochemical and isotopic evolution in the marine domain. We focus on two separated deltaic successions in the southern (Belsué locality, B) and northern (Yebra de Basa locality, YB) margins of the Jaca basin in the South-Pyrenean foreland basin (SPFB; Fig. 1). The successions are characterized by excellent exposure and have already been dated ~~thanks to~~by high-resolution magnetostratigraphy. Both sections reveal progradation of deltaic and fluvial systems coeval with the magnetic reversal occurring at chrons C18r and C18n.2n, near or at the zenith of MECO warmth (Edgar *et al.*, 2010, 2020; Garcés *et al.*, 2014; Vinyoles *et al.*, 2021). We generated new high-resolution profiles of $\delta^{13}C_{carb}$ ~~and~~, $\delta^{18}O_{carb}$, ~~XRF~~major and trace elements, ~~clays~~clay mineralogy, and ~~Rock~~ Rock-Eval parameters~~,~~ across the Chron C18r~~-~~–C18n.2n reversal~~, in order~~ ~~to~~ to identify geochemical changes associated with the MECO onset and its ~~recovery and~~recovery. We tested ~~test~~ the possible causative links between progradation and the MECO perturbation. Finally, we discuss the sedimentary evolution of both sections to understand landscape response during the MECO~~,~~ and explore~~and we explore~~ the significance of its identification in the SPFB and the impact of climate shifts in ~~source~~ source-~~to~~ to-sink systems as recorded at the continent~~-al to~~ ocean interface.

2 Geological ~~Setting~~setting

The Pyrenees are a nearly E-W trending mountain belt formed by the collision of the Iberian and European plates from the Late Cretaceous (Santonian) to the Early Miocene (Muñoz, 1992; Roure *et al.*, 1989; Teixell, 1998; Vergés *et al.* 2002). The south Pyrenean zone is composed of an imbricate system of synorogenic thrusted cover sheets propagating southwards, detached above the Triassic evaporites (Labaume and Teixell, 2018; Lagabrielle *et al.*, 2010; Mochales *et al.*, 2012; Pueyo, *et al.*, 2002; Teixell *et al.*, 2016, 2018). Among them, the emplacement of the South-Central Unit (SCU) by early Eocene resulted in the partition of the South Pyrenean Basin (SPFB) and the development of an E-W elongated deep basin draining west towards the Atlantic Ocean (Mochales *et al.*, 2012; Muñoz *et al.*, 2018; Puigdefàbregas, 1975, Puigdefàbregas and Souquet, 1986; Séguret, 1972). Due to the westward propagation of deformation during the middle Eocene and the differential velocity of the thrust sheets, oblique thrusted anticlines developed at the ~~south-~~southwestern ~~western~~ termination of the SCU (Muñoz *et al.*, 2013). These thrusts caused the fragmentation and piggy-back transport of a wider foreland region, which included from east to west: the Tremp-Graus, Ainsa, and eventually the Jaca basins (Muñoz *et al.*, 2018; Fig. 2).

The Tremp-Jaca basin (TJB) preserves an outstandingly exposed complete source-to-sink system during MECO times. In the middle Eocene, the alluvial-fluvial system of Sis-Escanilla flowed down the Tremp-Graus and Ainsa basins, draining the eroded sediments from the uplifting north~~h-~~eastern Pyrenees (Beamud *et al.*, 2003; Roigé *et al.*, 2016; Coll *et al.*, 2020; Puigdefábregas, 1975, 1986). Sediments were transported westwards into the Jaca basin, forming a mixed delta-carbonate

Con formato: Fuente: Cursiva
Con formato: Fuente: Cursiva
Con formato: Fuente: Cursiva
Con formato: Subíndice
Con formato: Fuente: Cursiva
Con formato: Fuente: Cursiva
Con formato: Fuente: Cursiva
Con formato: Fuente: Cursiva
Con formato: Fuente: Cursiva
Con formato: Fuente: Cursiva
Con formato: Fuente: Cursiva
Con formato: Fuente: Cursiva
Con formato: Fuente: Cursiva
Con formato: Fuente: Cursiva
Con formato: Fuente: Cursiva
Con formato: Fuente: Cursiva
Con formato: Fuente: Cursiva

ramp with tidal influence (Puigdefàbregas, 1975; Castelltort *et al.*, 2003). Two main deltaic systems developed during lower Bartonian in the southern (Belsué-Atarés) and northern (Sabiñánigo) margin of the Jaca basin~~n,~~ that primarily fed the distal Hecho turbidites in the western sector (Mutti, 1977; Remacha and Fernández, 1985). Shallow marine environments are mainly dominated by marly facies, ~~which~~ which, thanks to their high carbonate content ~~and the~~and relatively deep depositional ~~environment~~ environment, are suitable for geochemical ~~purposes~~ studies (Wendler, 2013). ~~Available h~~High-resolution magnetostratigraphy in the Pyrenean region ~~provides a correlation of~~correlates with different sections along the entire source-to-sink system (Vinyoles *et al.*, 2021). We selected two lower Bartonian sections, Belsué (BS) and Yebra de Basa (YB), because they present excellent exposition and are provided with magnetostratigraphic dating, aiming to unravel the geochemical history of the two main deltaic systems coeval to the MECO.

Con formato: Fuente: Cursiva

Con formato: Fuente: Cursiva

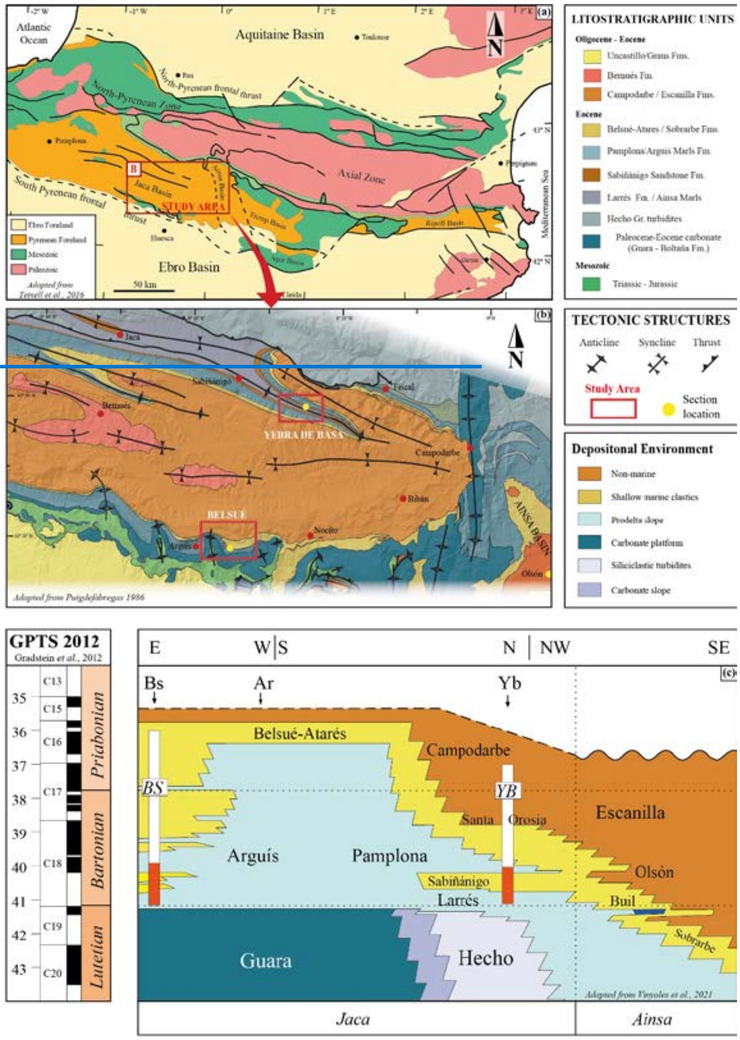

Atlantic Ocean
Aquitaine Basin
North-Pyrenean frontal thrust
North-Pyrenean Zone
Axial Zone
South Pyrenean frontal thrust
STUDY AREA
Ebro Basin
Ebro Foreland
Pyrenean Foreland
Mesozoic
Paleozoic
Adapted from Teixell et al., 2016
50 km
Mediterranean Sea
LITOSTRATIGRAPHIC UNITS
Oligocene - Eocene
Uncastillo/Graus Fms.
Bernués Fm.
Campodarbe / Escanilla Fms.
Eocene
Belsué-Atares / Sobrarbe Fms.
Pamplona/Arguis Marls Fm.
Sabiñánigo Sandstone Fm.
Larrés Fm. / Ainsa Marls
Hecho Gr. turbidites
Paleocene-Eocene carbonate (Guara - Boltaña Fm.)
Mesozoic
Triassic - Jurassic
TECTONIC STRUCTURES
Anticline
Syncline
Thrust
Study Area
Section location
Depositonal Environment
Non-marine
Shallow marine clastics
Prodelta slope
Carbonate platform
Siliciclastic turbidites
Carbonate slope
Jaca
Sabiñánigo
Bernués
YEBRA DE BASA
Campodarbe
BELSUÉ
Arguís
Nocito
Bibán
AINSA BASIN
Olsón
Adapted from Puigdefàbregas 1986
GPTS 2012
Gradstein et al., 2012
35
36
37
38
39
40
41
42
43
C13
C15
C16
C17
C18
C19
C20
Priabonian
Bartonian
Lutetian
E
W|S
N | NW
SE
Bs
Ar
Yb
(c)
Belsué-Atarés
Campodarbe
BS
YB
Santa Orosia
Escanilla
Arguís
Pamplona
Sabiñánigo
Olsón
Larrés
Buil
Sobrarbe
Guara
Hecho
Adapted from Vinyoles et al., 2021
Jaca
Ainsa

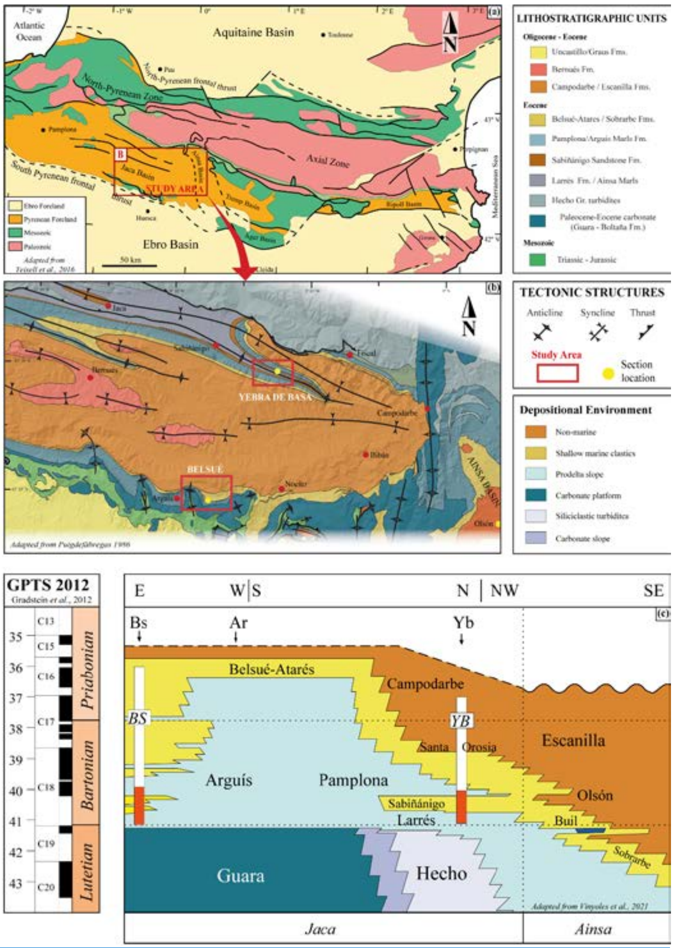

Figure 2: Geological and Stratigraphic context of the study area (a) Synthetic geologic map of the Pyrenees and location of the study area in the Jaca Basin (red square). Black lines represent the main tectonic structures. Modified from Teixell (1996) and Bosch (2016). (b) Detailed geologic map of the Jaca basin and the study area (Belsué and Yebra de Basa). Modified from Puigdefàbregas (1975) and Remacha (1996). (c) Chronostratigraphy of the Ainsa and Jaca basins, showing the westwards progradation of all depositional systems. The names of the main lithostratigraphic units are represented in black. The studied sections (in white) are included in the work of Vinyoles *et al*~~., .~~ (2021), ~~(in white) whilst~~while the location of the geochemical analyses carried out in this paper is highlighted in red. The figure is modified from Vinyoles *et al.* (2021).

Con formato: Fuente: Cursiva

Con formato: Fuente: Cursiva

The ~~130 m~~130 m thick BS section is located within the External Sierras, east of the "Pico del Águila" anticline (~~Fig. 3;~~ 42.30º N 0.37º W; Fig. 3). This section has been extensively studied as a perfect case study for the tectonic–sedimentation relationship (Fig. 2; ~~(~~Puigdefàbregas, 1975; Puigdefàbregas and Souquet, 1986; Millán *et al*., 1994, 2000; Castelltort *et al*., 2003; Huyghe *et al*., 2012; Garcés *et al*., 2014). The lower boundary corresponds to an encrusted and ferruginous surface on top of a shallow marine bioclastic limestone (Guara Fm.), locally overlain by sandy marls rich in glauconite (Millán *et al*., 1994). It has been interpreted as a drowning unconformity of the Guara carbonate platform (Puigdefàbregas, 1975; Silva-Casal *et al*., 2019), close to the Lutetian-Bartonian boundary (Rodriguez Pintó *et al*., 2013). This major unconformity led to the syntectonic deposition of the Arguís marls and the Belsué sandstones, while the Gabardiella and Pico del Águila anticlines were growing. Different authors studied the influence in the stratigraphy of local tectonic movement in Belsué-Arguís region (Lafont, 1994; Castelltort *et al*., 2003), concluding that local tectonics modify the stacking pattern and position of its genetic units along with different depositional environments. The entire section covers the lower Bartonian interval (Garcés *et al*., 2014) up to a maximum flooding surface MFS–2 by Muñoz *et al*. (1994~~;~~) (Fig. 3), which corresponds to the deepest paleobathymetry in the BS area (*ca*. 150 m, Sztràkos and Castelltort, 2001).

Con formato: Fuente: Cursiva

Con formato: Fuente: Cursiva

Con formato: Fuente: Cursiva

Con formato: Fuente: Cursiva

Con formato: Fuente: Cursiva

Con formato: Fuente: Cursiva

Con formato: Fuente: Cursiva

Con formato: Fuente: Cursiva

Con formato: Fuente: Cursiva

Con formato: Fuente: Cursiva

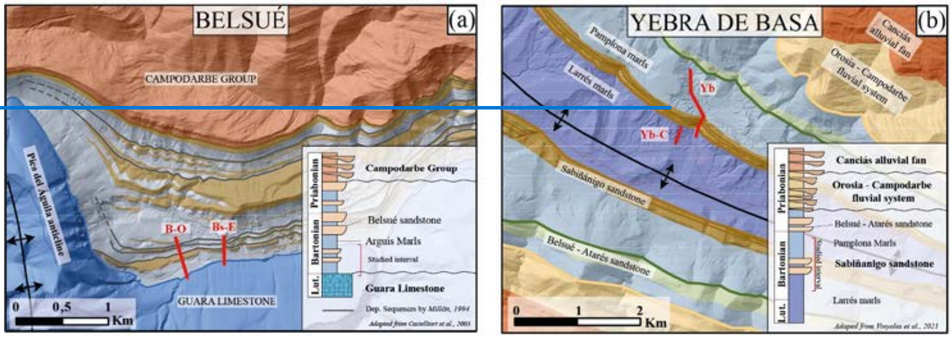

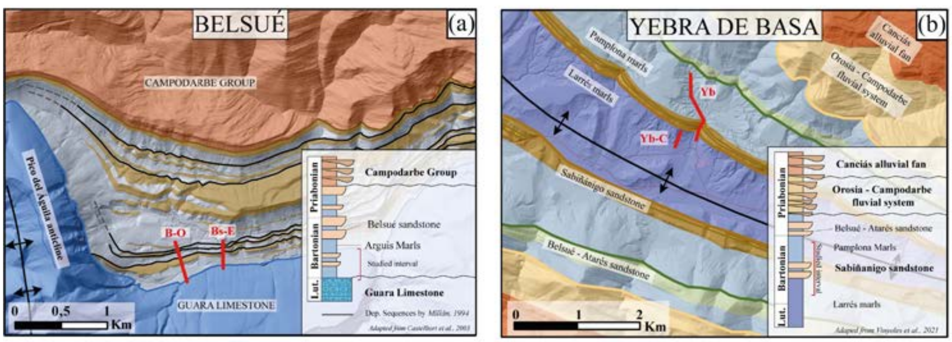

Figure 3. Detailed ~~geologic~~ geological maps from Belsué (a) and Yebra de Basa (b), modified respectively from Puigdefàbregas (1975) and Remacha (1996). ~~Small stratigraphic logs on the bottom right represent large-scale synthetic logs representing the different formations name, which are modified from Vinyoles *et al.* (2021) for Yebra de Basa and Castelltort *et al.* (2003) for Belsué.~~ Red lines ~~represent~~ show the location of the studied ~~sections locations~~sites, and the darker grey lines in Belsué represent the depositional sequences defined by Millán *et al.* (1994). Small stratigraphic logs on the bottom right represent large-scale synthetic logs with the formations name, which are modified from Vinyoles *et al.* (2021) for Yebra de Basa and Castelltort *et al.* (2003) for Belsué.

The ~~800 m~~800 m YB section is located between the Basa anticline and the Santa Orosia syncline (~~Fig. 3;~~ 42.49º N 0.28º W; Fig. 3~~), and~~) and comprises one of the best outcropping sections for the Sabiñánigo sandstone (Puigdefàbregas, 1975; Lafont, 1994; Boya, 2018). It is composed of three subsections covering the lower Bartonian interval, ~~(Fig. 3),~~ between the upper part of the chron C18r and the chron C18n.1r (Vinyoles *et al.*, 2021). The first subsection is located west (Yb-C), within the Larrés marls, whose top is correlated with the base of the Vinyoles *et al.*, (2021) magnetostratigraphic profile. From here, the next two subsections were built following the Vinyoles *et al.* (2021) profile, which comprises the two deltaic levels of the Sabiñánigo sandstone and most of the overlaying Pamplona marls.

Con formato: Fuente: Cursiva

Con formato: Fuente: Cursiva

Con formato: Fuente: Cursiva

Con formato: Fuente: Cursiva

3 Materials and methods

3.1 Field and sampling

We performed a complete stratigraphic study and sampling of the lower Bartonian sections from BS and YB. The stratigraphic thickness of these sections was measured using the Jacobs staff in the field and geometric calculations when direct measurements were impossible. New mapping based on fieldwork and orthophotos was performed to correlate the different subsections. The Belsué section in the southern margin is composed of two subsections (Fig. 3); the lower one (BS-E) was sampled at a resolution of 0.5–1.0 m and the upper one (BS-O) every 3–6 m. In the northern margin, the higher average sedimentation rate (SR) in Yebra de Basa (>80 cm/kyr; Vinyoles *et al.*, 2021) motivated a high-resolution sampling of 1–3 m at the middle part of the section (YB-HR~~), and~~) and ~~sampling~~ each 9–15 m in the other intervals (YB-C and YB-sup).

A total of 101 samples in BS and 157 samples in YB were collected~~, each~~. Each ~~of them~~ was composed of~~by~~ *ca.* 200 g of fine-grained and fresh ~~rock from~~rock below the weathering depth to avoid alteration and grain size bias (e.g., Lupker *et al.*, 2011). The samples were mostly marls, ~~which correspond~~corresponding to rocks rich in carbonate, ~~organic matter~~OM, and clays. These samples were prepared for mineralogical and geochemical analyses in the laboratories of the University of Geneva and the University of Lausanne. The sample surface was cleaned with deionized water, the weathered material was removed, and then dried at 45ºC for 2–3 days. The dried samples were crushed with a hydraulic press and powdered using an agate mill. The exposure conditions were usually ideal for sampling in both sections. ~~Still,~~However, there were ~~, but~~ difficulties ~~occurred~~ in four intervals, resulting in gaps in the data. ~~(data gaps) because of~~The problems were due to ~~either 1)~~ a dominance in sandy facies at the outcrop, corresponding to moments of maximum deltaic progradation, or ~~2)~~to ~~insufficient~~poor exposure ~~due to~~because of the fine-grained nature of the marls (e.g., Quaternary cover).

3.2 Clay ~~Mineralogy (XRD~~mineralogy~~)~~

The clay ~~mineralogical~~ mineral assemblages of 24 representative samples per section were determined by X-ray diffractometry. The used system was a Thermo Scientific ARL X-TRA diffractometer at the Institute of Earth Science of the University of Lausanne (ISTE-UNIL), following the methods described by Klug and Alexander (1974), Kübler (1983, 1987) and Adatte *et al.* (1996). Ground chips were mixed with deionized water (pH 7~~ to ~~–8) and agitated. The carbonate fraction was removed by treatment with 10% HCl at room temperature and then for 20 minutes or more until all carbonate was dissolved. The insoluble residue was disaggregated (ultrasonication, 3 min), washed and centrifuged (8 times) until a neutral suspension was obtained (pH 7–8). Different grain size fractions (<2 to 16 μm) were separated by the time settling method based on Stokes law. The selected fraction was then pipetted onto a glass plate and air-dried at room temperature. XRD analyses of oriented clay samples were made after air drying at room temperature at ethylene-glycol-solvated conditions. The intensities of XRD peaks (2θ~~,~~; Moore and Reynolds, 1997) characteristic of each clay mineral (*e.g.*, chlorite, mica, kaolinite) were used for a semi-quantitative estimation of the relative percent of clay minerals present in two size fractions (<2 μm and 2–16 μm).

Con formato: Fuente: Cursiva

Con formato: Fuente: Cursiva

Con formato: Fuente: Cursiva

Con formato: Fuente: Cursiva

3.3 Major and trace element ~~composition~~compositions ~~(XRF)~~

Major and trace element concentrations from 24 representative samples per section were determined by X-ray fluorescence (XRF) spectrometry, using a PANalytical PW2400 spectrometer from ISTE-UNIL. The major elements were analysed ~~from a~~on fused glass discs. First, ~~To prepare them between~~ 2.7 to 3 g of sample powder was ~~put~~ heated in a crucible oven at ~~t (~~1050ºC~~)~~ ~~for~~ for one night~~t, and then weighted~~ ~~to~~ to obtain the ~~Loss of Ignition~~loss on ignition (LOI) value. ~~This~~ Then, 1.2000 ± 0.0005 g of the calcinated ~~samples~~ sample ~~were~~ was mix with 6.0000 ± 0.0005 g ~~then used for preparing the fused~~ lithium tetraborate ($Li_2B_4O_7$~~)~~) to prepare the fused glass disc using an ~~. To prepare them, we need to weight 6.0000g ± 0.0005g of lithium tetraborate and 1.2000g ± 0.0005 of calcinated sample. Both were put in an agate mortar and pound for 3 minutes to obtain a homogenised powder. The powder was poured in a platinum crucible and in the~~ automated glass bead-casting machine ~~at University of Geneva~~ (Pearl-X'3) at the University of Geneva.~~) to obtain a glass disc.~~

The trace elements were analysed using~~from a~~ ~~pressed disc~~pressed powder discs~~, assembled by weighting~~ prepared at the University of Geneva from 3.000~~g~~ ± 0.0005 g of wax and 12.000~~g~~ ± 0.0005g of non-calcinated sample powder. The mixture was ~~poured in a closed plastic container and shaken for 3 minutes to obtain a~~ homogenised ~~powder. The powder was then poured in~~and pressed~~ a hydraulic press~~ ~~and (1 tonne~~1 ton hydraulic ~~of~~ press~~ure,~~ ~~was applied on it during approximately~~ 20 seconds~~, performed) at University of Geneva~~. Accuracy of the ~~analysed discs~~XRF analyses, assessed by analyses of standard reference materials, ~~is~~ was 0.4 wt.% for the major elements and 1 to 3 ppm for the trace elements~~, assessed by analyses of standard reference materials~~.

3.4 Rock-Eval pyrolysis

The quality and quantity ~~of preserved~~of the organic matter (OM) were determined in 237 bulk rock powders using ~~the equipment~~a Rock-Eval 6 instrument at ISTE-UNIL~~ISTE – UNIL~~, following the method described by Behar *et al*. (2001) and using the IFP 160000 standard. Aliquots of samples were placed in an oven~~, and first heated~~heated at 300ºC under an inert atmosphere, and then gradually pyrolyzed up to 650 °C. After the ~~pyrolysis was complete~~pyrolysis, the samples were transferred into another oven and gradually heated up to 850°C in the presence of air, analysing the CO_2 and hydrocarbon (HC) concentration during ~~all the~~ the entire process. The calculated parameters included total organic carbon content (TOC, wt.%), hydrogen index (HI~~,~~ in mg HC/g~~$^{-1}$~~ TOC), oxygen index (OI~~,~~ in mg CO_2/g~~$^{-1}$~~ TOC), and T_{max} (ºC) according to Espitalié *et al*. (1985) and Behar *et al*. (2001).

3.5 Carbonate carbon and oxygen stable isotopes

Carbonate carbon and oxygen stable isotope ~~analysis~~ ratios ($\delta^{13}C_{carb}$ and $\delta^{18}O_{carb}$) of whole rock powders containing > 10 wt.% $CaCO_3$ (*n* = 237) were ~~performed~~ determined at ~~the~~ the ~~stable isotope~~ laboratories of the Institute of Earth Surface Dynamics of the University of Lausanne (IDYST-UNIL~~).~~) using a ~~The used equipment was a~~ Thermo Fisher Scientific Gas Bench II carbonate preparation device connected to a Delta Plus XL isotope ratio mass spectrometer ~~a Delta Plus XL isotope ratio mass~~

Con formato: Fuente: Cursiva

Con formato: Fuente: Cursiva

Con formato: Fuente: Cursiva

~~spectrometer~~. The CO_2 extraction was done by reaction with phosphoric acid at 70°C. ~~The stable~~The carbon and oxygen stable isotope ratios were reported in the delta (δ) notation as the per mil (‰) relative to the Vienna Pee Dee belemnite standard (VPDB), where $\delta = (R_{sample} - R_{standard})/R_{standard} \times 1000$ and $R = {}^{13}C/{}^{12}C$ or ${}^{18}O/{}^{16}O$. The $\delta^{13}C_{carb}$ and $\delta^{18}O_{carb}$ values were standardized relative to the international VPDB scale by calibration of the reference gases and working standards with the international reference materials NBS 18 (carbonatite, $\delta^{13}C$ = –5.04 ‰, $\delta^{18}O$ = –23.00 ‰) and NBS 19 (limestone, $\delta^{13}C$ = +1.95 ‰, $\delta^{18}O$ = –2.19 ‰). Analytical uncertainty (1 sigma), monitored by replicate analyses of the international calcite standard NBS 19 and the laboratory standard Carrara Marble ($\delta^{13}C$ = +2.05 ‰, $\delta^{18}O$ = –1.7 ‰), was not greater than ±0.05‰ for $\delta^{13}C$ and ±0.1 ‰ for $\delta^{18}O$.

3.6 Organic ~~Carbon~~ carbon stable isotopes

The organic carbon stable isotope ratios ($\delta^{13}C_{org}$ values in ‰ vs. VPDB) were determined in 155 samples, which were previously decarbonated by treatment with 10% v/v HCl, thoroughly washed with deionized water and dried (40 °C, 48 h). The $\delta^{13}C_{org}$ measurements were performed at the IDYST-UNIL by elemental analysis/isotope ratio mass spectrometry, using a Carlo Erba 1108 (Fisons Instruments, Milan, Italy) elemental analyzer connected to a Delta V Plus isotope ratio mass spectrometer via a ConFlo III split interface (both of Thermo Fisher Scientific, Bremen, Germany) operated under continuous helium flow (Spangenberg and Herlec, 2006). The calibration and normalization of the measured $\delta^{13}C$ to the VPDB scale was performed with international reference materials and UNIL in-house standards (Spangenberg and Herlec, 2006; Spangenberg, 2016). The repeatability and intermediate precision were better than 0.1 ‰ for $\delta^{13}C_{org}$.

4 Results

4.1 Stratigraphy and sedimentology

Belsué (BS) stratigraphic succession records the interfingering between prodelta (Arguís Fm.) and deltaic sediments (Belsué Fm.). The Arguís Fm. are highly bioturbated marls and silts, often rich in glauconite, with sparse bioclasts (*e.g.*, ~~-~~ bivalves~~),~~) and oxidized ~~organic matter (OM)~~OM fragments. Sandstone beds (Belsué Fm.) are interlayered within the marls, forming two major coarsening and thickening upwards sequences that consist of medium sandstone beds (5~~–~~–10 m thick~~),~~) with sharp erosion base, parallel stratification, undifferentiated ripples, and glauconite rich horizons (Fig. 4). The Arguís marls are interpreted as prodelta deposits in a poorly circulated and relatively deep marine environment (Millán *et al*., 1994). The marls prelude deltaic mouth bars (Belsué Fm.) where the fluvial component predominates, although local effects from storms and tides are observed (Millán *et al*., 1994; Castelltort *et al*., 2003). Calculated paleocurrents show a corrected east/south-east sediment supply source, in agreement with previous studies (Puigdefàbregas, 1975; Lafont, 1994; Millán *et al*., 1994; Garcés *et al*., 2014). Both formations are interpreted as a mixed delta-carbonate ramp system prograding ~~westward~~ westward, spanning from Bartonian to Priabonian (Castelltort *et al*., 2003).

Con formato: Fuente: Cursiva

Con formato: Fuente: Cursiva

Con formato: Fuente: Cursiva

Con formato: Fuente: Cursiva

Con formato: Fuente: Cursiva

Con formato: Fuente: Cursiva

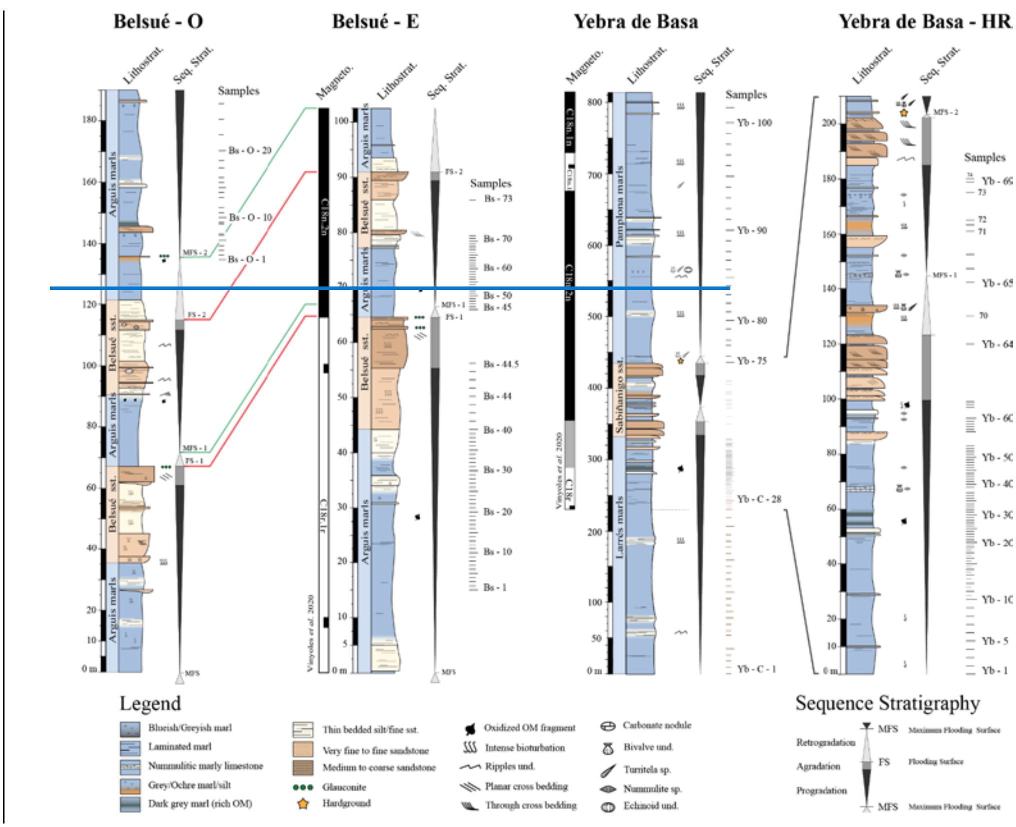
Belsué - O
Belsué - E
Yebra de Basa
Yebra de Basa - HR
Magneto.
Lithostrat.
Seq. Strat.
Samples
Arguis marls
Belsué sst.
Pamplona marls
Sabiñanigo sst.
Larrés marls
MFS - 2
MFS - 1
FS - 2
FS - 1
MFS
Vinyoles et al. 2020
Legend
Blueish/Greyish marl
Laminated marl
Nummulitic marly limestone
Grey/Ochre marl/silt
Dark grey marl (rich OM)
Thin bedded silt/fine sst.
Very fine to fine sandstone
Medium to coarse sandstone
Glauconite
Hardground
Oxidized OM fragment
Intense bioturbation
Ripples und.
Planar cross bedding
Through cross bedding
Carbonate nodule
Bivalve und.
Turritela sp.
Nummulite sp.
Echinoid und.
Sequence Stratigraphy
Retrogradation
Agradation
Progradation
MFS Maximum Flooding Surface
FS Flooding Surface
MFS Maximum Flooding Surface

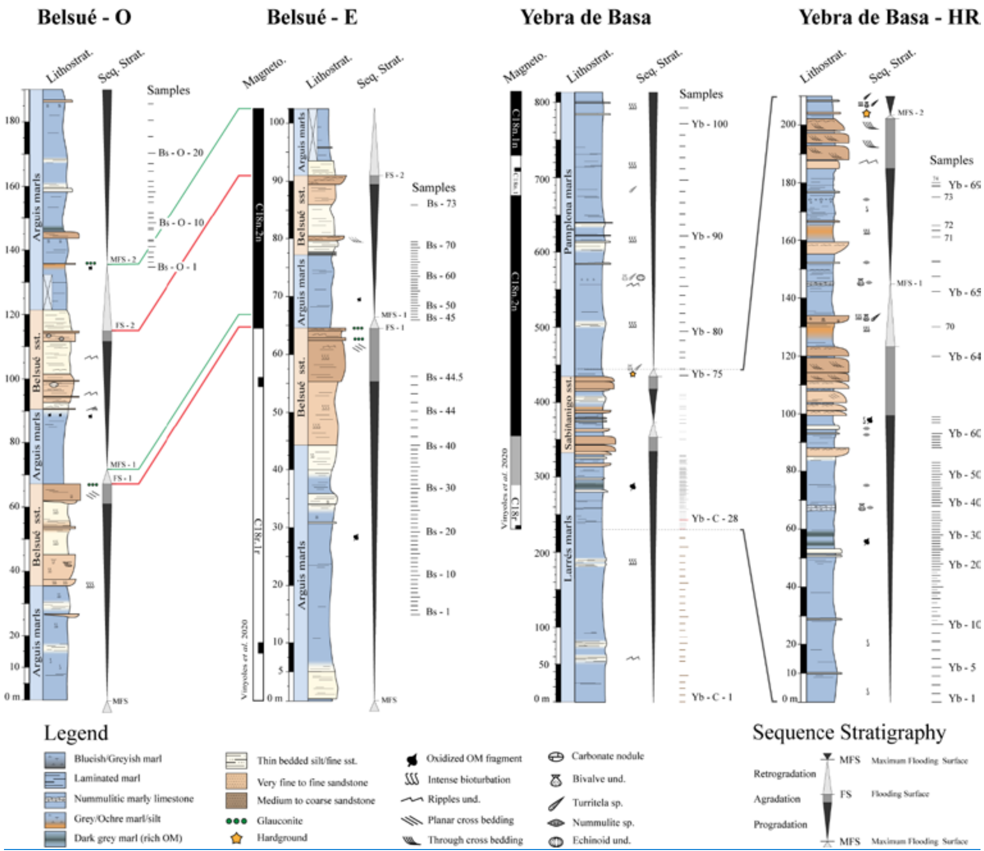

Figure 4: Stratigraphic logs of Belsué – East (BS-E), Belsué – West (BS-O), and Yebra de Basa, with a more complete high-resolution log (Yebra de Basa – HR). Red lines represent flooding surfaces (FS) and green lines the maximum flooding surfaces (MFS) correlation. Facies interpretation of the sedimentary logs are represented by grey bars, being more proximal the grey bar and more distal the white. Abbreviations used: Magneto. for magnetostratigraphy, Lithostrat. for lithostratigraphy; and Seq. Strat. for Sequence stratigraphy. The poor exposure zones in Belsué are covered with a semi-transparent white rectangle with a black cross.

On the northern margin of the basin, the Yebra de Basa (YB) section starts with laminated blue marls (Larrés Fm.) that are interlayered by sparse siltstone beds and two dark levels rich in ~~organic matter~~OM (56-–60 m in Yebra-HR). The Larrés Fm. transitions to the Sabiñánigo sandstone (SS~~),~~), ~~that is~~ composed ~~by~~ of two thickening and coarsening upwards sequences. The sandstone beds present planar and through cross-stratification~~,~~ erosion scours, ~~as well as~~ sigmoidal ~~beds~~ beds, and flasser-wavy stratification. The upper boundary (*ca.* 205 m in ~~Yebra~~ Yebra-HR) is marked by a sharp contrast towards a highly bioturbated and fossiliferous horizon (hard-ground), leading to the deposition of laminated grey-blue marls (Pamplona Fm.), less interlayered with siltstones beds, but richer in fossiliferous horizons (Turritella *sp.* mainly). The system is interpreted as a deltaic siliciclastic shelf prograding W-SW (Roigé *et al*., 2018), defined as a fluvial delta with local tidal rework. The deltaic system ended abruptly with a major flooding that thatthat formed a hard hard ground and led to the Pamplona prodelatic marls deposition (Lafont, 1994; Puigdefàbregas, 1975).

As mentioned in section 3.1, although the exposure conditions were greatexcellent for sampling, we had four intervals (data gaps) without a continuous sampling, leading to local data gaps. and threeThree of these data gaps of them are becausewere due to ofthe dominance inof sandy facies. In YB, the sandy intervals correspond to the Sabiñánigo sst.sandstone deltaic bodies located approximately betweenat ~100 to ~120 m and ~180 to ~200 m (YB-HR section; Fig. 4),. whereas inIn BS, the Belsué sst.sandstone interval is placed between ~55 and ~60 m (Belsué-E section; Fig. 4). The fourth data gap,The fourth data gap located betweenat ~85 to ~ 115 m in Belsué-E, results of lack of sufficient exposure within the marls and alsoand the presence of a coarse-grained sandy interval (Fig. 4).

Facies associations were described by combining the observations in the field and the availableand information by severalfrom previous studies in the Jaca basin (Millán *et al*., 1994; 2000; Castelltort *et al*., 2003; Lafont, 1994; Puigdefàbregas, 1975; Boya, 2018). Using the vertical variations of facies in our the studied sections, we defined the depositional sequences that record the cycles of the shoreline's shoreline progradation/ and retrogradation (P-R) cycles. Here, we used the smallest correlatable sequences, which are termed parasequences when bounded by the two shallowest facies (flooding surface, FS, ; van Wagonerr, *et al*., 1988, 1990), or genetic units when bounded by the two deepest facies (maximum flooding surface, MFS, ; Homewoodd, *et al*., 1992). The sequence stratigraphic interpretation is summarized in Fig. 4, where parasequences thickness from Belsué and Yebra de Basa vary from a few to tens of meters (5 to –50 m), and its stacking pattern defines two main P-R cycles in both sections.

4.2 Clay Mineralsmineralogy

In both sections, Belsué and Yebra de Basa, more than 90% of the total recorded clay mineral assemblage correspond to the sum of Chloritechlorite, Chloritechlorite/Smectite smectite (CS), Micamica, or Illiteillite/Smectite smectite (IS) (Fig. 5). This association of clay minerals is characteristic of dominant physical erosion (Adatte *et al*., 2000). Mica is the most common clay in both sections (40% to –65%), followed by Chlorite chlorite (10 to –36%). In contrast, the percentage of Kaolinite kaolinite is very low (<5%). In Belsué, both progradations show different Chlorite chlorite concentrationscontents, being higher in the upper part. At Yebra de Basa, we observe an increase in Mica mica that coincides with the OM peak. The absence of smectite indicates it has been transformed during diagenesis into CS or IS mixed layers during diagenesis, . and itsIts percentage, 20––30% in our the studied sections, can be used as a burial estimation (Kübler, 2000). Kaolinite is content positively correlated correlates with the deltaic progradation, indicating that kaolinite could be predominantly mainly transported.

Con formato: Fuente: Cursiva
Con formato: Fuente: Cursiva
Con formato: Fuente: Cursiva
Con formato: Sin Resaltar
Con formato: Fuente: Cursiva
Con formato: Fuente: Cursiva
Con formato: Fuente: Cursiva

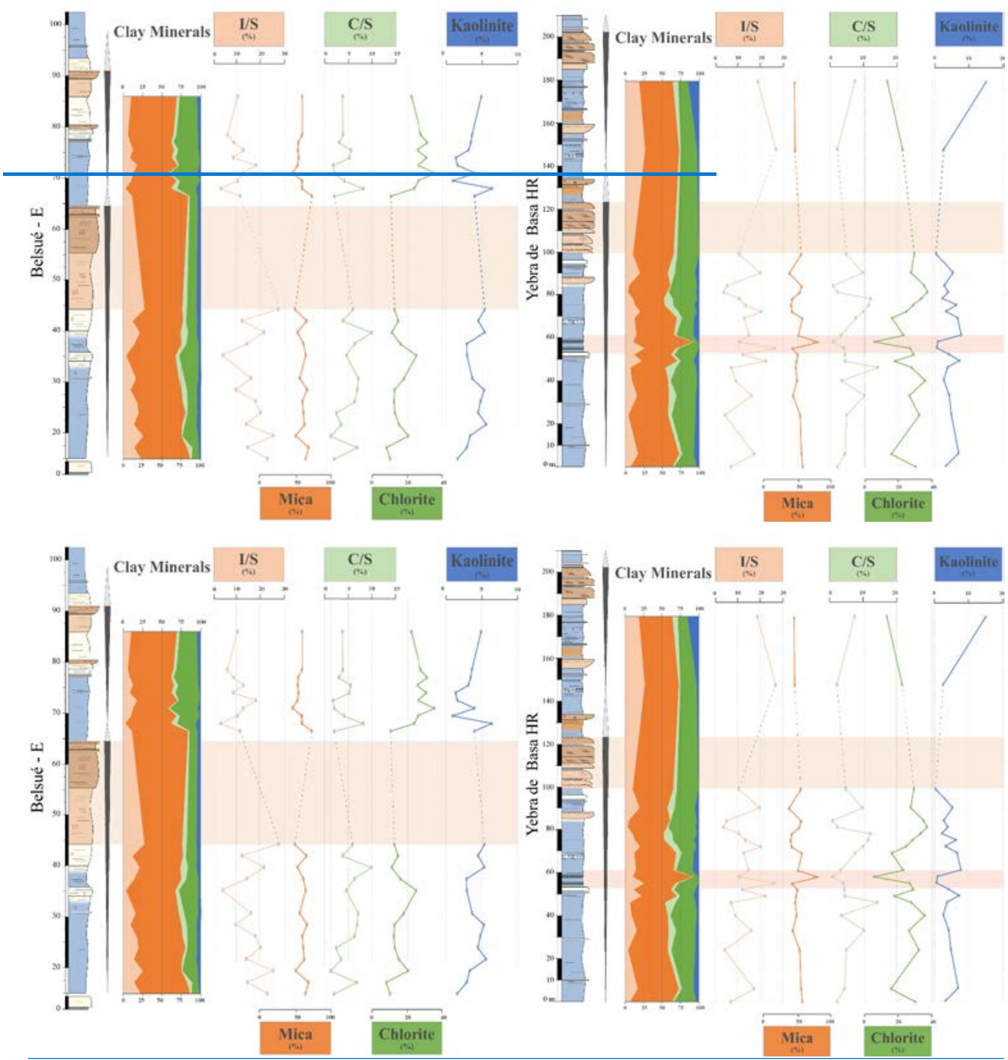

Figure 5: Schematic stratigraphic log of Belsué-E (left) and Yebra de Basa – HR (right) with clay mineral assemblages, I/S (illite/smectite), C/S (cChlorite/sSmectite), mica, cChlorite, I/S (Illite/Smectite), Mica or Illite and Kaolinitekaolinite. Highlighted in pale red is the organic OM-rich interval in Yebra de Basa, and in pale brown are the main sandstone levels. The progradation-retrogradation cycles (P-R) are drawn with grey and white triangles. The dashed lines represent non-sampled intervals.

4.3 Geochemistry

4.3.1 Major and trace elements

The major and trace elements have been normalized to aluminium (Al) to limit the dilution effect caused by different proportions of terrigenous sediment components (van der Weijden *et al*., 2002; Fig. 6). At BS, two increasing pulses of detrital major (Si, Fe, K, and Ti) and trace elements (Mn, and Sr) are concomitant with both deltaic progradations (Fig 6). The similar trend of cCalcium (Ca) (Ca) suggests an extrabasinal origin, likely from the eroded Mesozoic or Palaeocene carbonate platforms. Only the potassium (K)K show shows a negative trend compared to the detrital elements, likely related to clay abundance. At YB, the high TOC interval (depicted in red in Figure 6) coincides with a relative decrease of the major Si, Ca, Ti, and K, and the trace Sr, Zr Zr, and Sn, normalized to aluminiumAl. In contrast, the OM-related elements increase, such as the V/Cr ratio, which is related with to organic matterOM-rich and suboxic/anoxic conditions (van der Weijden *et al*., 2006), or the Ni/Co ratio, which is related to biogenic production (Tribovillard *et al*., 2006).

Con formato: Fuente: Cursiva

Con formato: Fuente: Cursiva

Con formato: Fuente: Cursiva

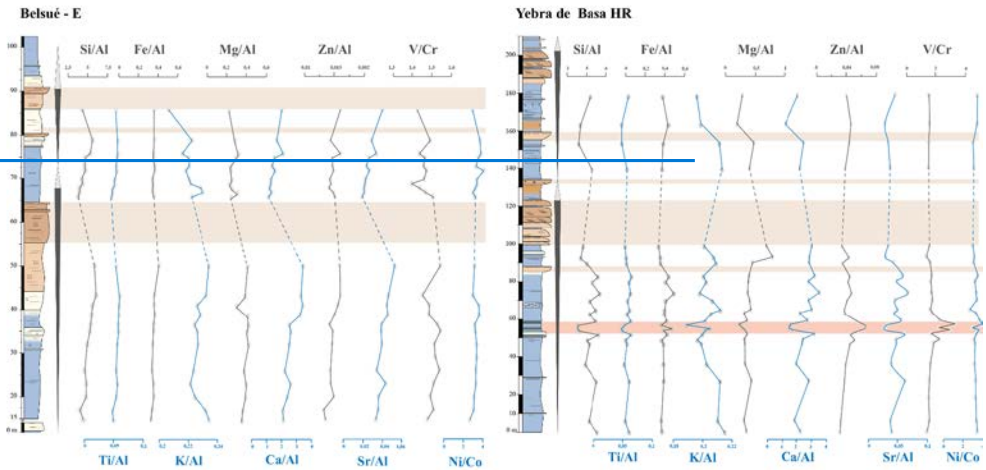

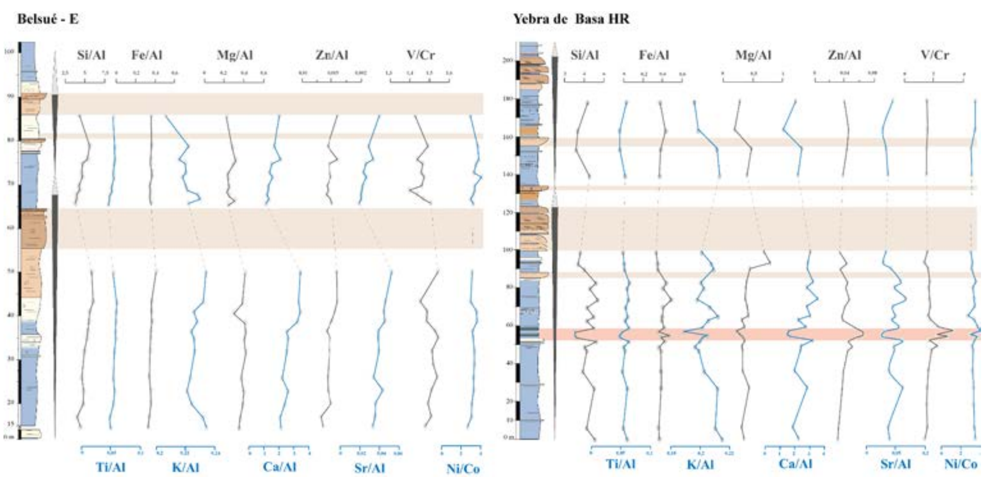

Figure 6: Stratigraphic profiles of Belsué - E and Yebra de Basa HR with the normalized major element concentrations (Si, Fe, Mg, Ti, and K), trace ~~elements~~ element concentrations (Sr~~,~~ and Zn), and trace element ratios (Ni/Co, V/Cr, and ~~and~~ U/Th). The progradation-retrogradation cycles (P-R) are drawn with grey and white triangles. ~~Highlighted~~ They are highlighted in pale brown de sandstone levels~~,~~ and in ~~in red~~red the ~~organic matter~~OM~~-~~-rich interval in Yebra de Basa. ~~The progradation-retrogradation cycles (P-R) are drawn with grey and white triangles.~~ The dashed lines represent non-sample intervals.

~~4.4 Geochemistry~~

Con formato: Resaltar

4.4~~3.2.1~~ Organic matter content, type, and evaluation

~~The overall~~The total organic carbon content (TOC) is low in both sections (average <0~~,~~.5 wt. %; Fig. 7). At BS, the TOC values range from 0.06 to 0.38 % (average 0.2 ± 0.07 wt. %). The lower one shows a decreasing trend of TOC that follows the deltaic progradation, showing that the OM concentrations decrease with increasing clastic material ~~the OM concentration decrease~~. The upper section also depicts this trend, with~~, and~~ the higher and more stable TOC values (~~~0,~~0.3 wt.%) ~~that are associated with~~within marly prodelta deposits. ~~In the other hand~~Conversely, YB TOC values range from 0.14% to 1.3% (average 0.3 ± 0.13 wt. %). The most prominent feature is a dark-grey marl interval ~~(Fig. 7)~~ with a ~~organic matter~~TOC ~~peak~~ spike ~~that reaches values higher than~~of ~~-~~>1 wt.~~%, and~~%, which is ~~is~~ associated with ~~a~~ negative carbonate carbon and oxygen ~~isotopic~~ isotope excursions (Fig. 7). Apart from this ~~major~~ significant excursion, most TOC values ~~values keep~~are close to 0.3% wt.% and no other ~~major~~ significant variations ~~occur~~ along the page section. In the high-resolution part of the section, there are small oscillations varying up to ±0.1 wt.%.

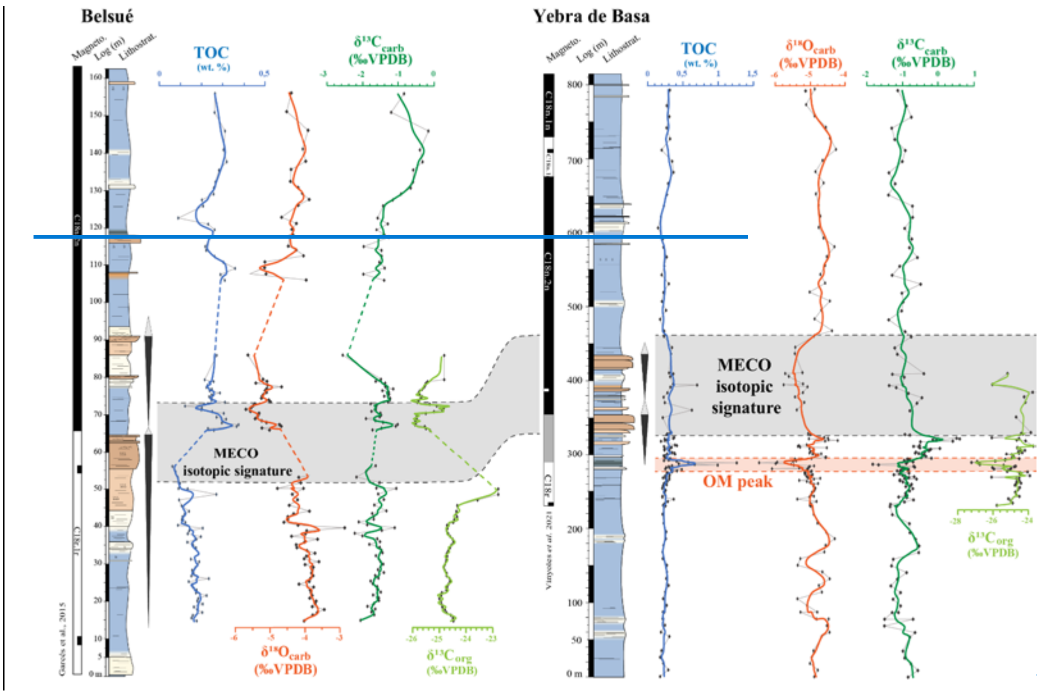

Belsué
Yebra de Basa
Magneto.
Log (m)
Lithostrat.
TOC
(wt. %)
δ¹³Ccarb
(‰VPDB)
δ¹⁸Ocarb
(‰VPDB)
δ¹³Corg
(‰VPDB)
MECO
isotopic signature
OM peak
Garcés et al., 2015
Vinyoles et al. 2021

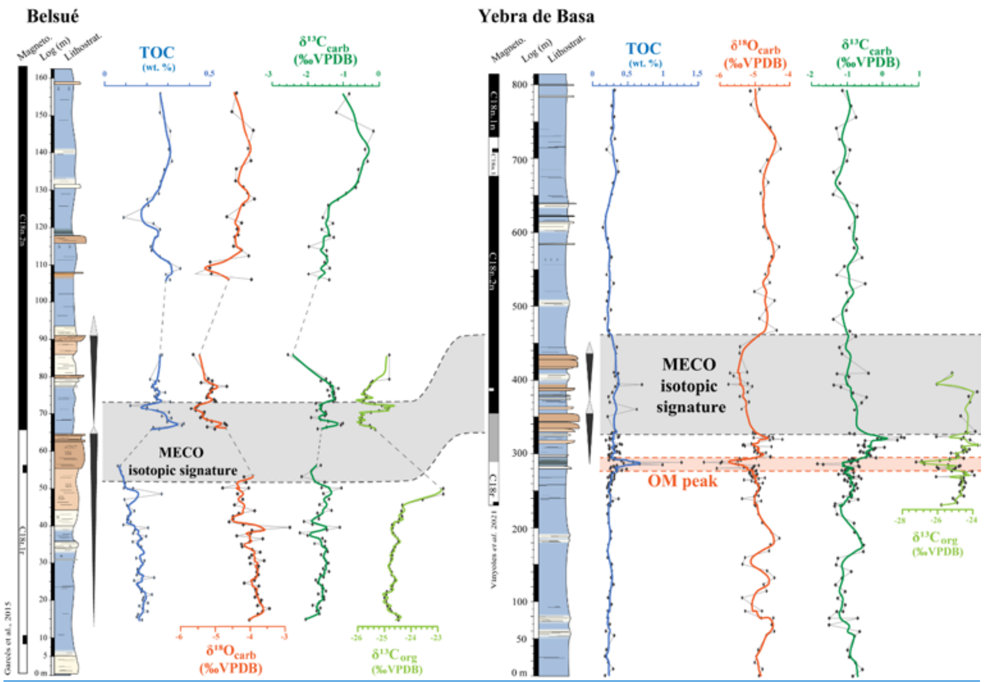

Figure 7: Stratigraphic logs of Belsué and Yebra de Basa including the results of total organic carbon (TOC~~C wt.%~~), ~~stable~~ carbonate stable isotopes ($\delta^{18}O_{carb}$ and $\delta^{13}C_{carb}$), and organic carbon stable isotopes ($\delta^{13}C_{org}$). The two progradation-retrogradation cycles referred to in the text are drawn next to the stratigraphy~~,~~; note the scale change ~~in the scale~~. Highlighted in grey is the MECO isotopic signature and in pale red ~~are the~~the OM-rich interval coeval to the MECO thermal peak. The ~~wide~~ coloured broad lines correspond to the 3-point moving average~~,~~; whilst the central part of the Yebra de Basa section ~~due to its high resolution has~~ has a 7-point moving average curve, due to the high sampling resolution. Magnetostratigraphic logs from ~~-~~Vinyoles et al.~~,~~ (2021) and Garcés et al.~~,~~ (2015). The dashed lines represent non-sample intervals.

Con formato: Inglés (Reino Unido)

The ~~values of~~ T_{max} values and the ~~classify the~~ HI (Hydrogen Index)/OI (Oxygen Index) ratios serve to classify the ~~in terms of~~ OM in terms of ~~origin and quality~~type (origin) and thermal maturity (Espitalié *et al*., 1985). ~~Our results show that samples~~The T_{max} values of the samples range ~~from~~ between 422 and~~ºC to~~ 445ºC (Fig. 8), with some exceptions reaching almost 460ºC. This indicates that the character of the preserved OM is generally immature or within the oil ~~zone~~ window (Fig. 8). The ~~hydrogen index (HI)~~HI values in YB and BS ~~is~~ are generally ~~below~~ ≤100 mg HC/g TOC (average 65 mg HC/g TOC), ~~which falls in~~corresponding to OM of ~~Type~~ types III and ~~Type~~ IV ~~zone of organic matter origin~~, ~~characteristic~~ indicative of a high input of terrestrial plants (Espitalié et al., 1985, Fig. 8). Some samples in Belsué (BS-W) ~~record higher~~have HI ≥~~than~~ 150 mg HC/g TOC, ~~this~~ which is probably related with a slightly different depositional condition between the sections (more distal in the W). The ~~oxygen index (OI)~~OI values show~~s~~ a similar trend ~~than~~ to the HI values, ~~keeping~~having ~~-~~ values below 100 mg CO_2/g TOC (average 82 mg CO_2/g TOC), but more dispersed than HI values. In summary, the Rock-Eval parameters indicate

Con formato: Fuente: Cursiva

Altogether points out towards a recycled source and/or terrestrial origin of the organic matter in both sections (OM, for both YB and BS sections).

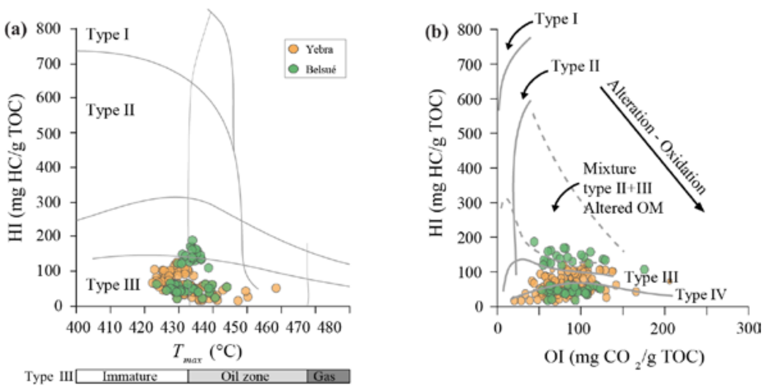

Figure 8: (A) The scatter plot of hydrogen index (HI) vs. T_{max} values allows to discriminate the different kerogen types, (B) whereas the scatter plot of hydrogen (HI) vs., oxygen index (OI) allows to assess the OM sourceorigin and thermal maturity. Here we display the kerogen types (A) and the OM origin (B) from Yebra de Basa (orange) and Belsué (green). Samples with lower TOC values lower than 0,.2 wt.% have been excluded. Reference lines for kerogen types and maturity based onafter Espitalié (1986).

4.43.2 3 Carbonate carbon and oxygen stable isotopes

At BS, the $\delta^{13}C_{carb}$ values range from -2.6 to -0.2 ‰ (-1.5 ± 0.4 ‰), ‰) and the $\delta^{18}O_{carb}$ values range from -5.7 to -2.9 ‰ (average -4.4 ± 0.6 ‰; Fig. 7). Oxygen isotope ratiosThe $\delta^{18}O_{carb}$ values show a gradual decreasing trenddecrease (of -1.5 ‰) during the first two deltaic progradations (-1.5 ‰), coinciding with a very gradual and small positive trend of the $\delta^{13}C_{carb}$. values. After the second progradation, $\delta^{18}O_{carb}$ rapidly returns to more positive values, which are maintained until the top of the section. This steadiness is not followed by the $\delta^{13}C_{carb}$ results values, which rthat record a pronounced positive shift of +1 ‰ between 125 and 150 m height. (+1 ‰). The $\delta^{18}O_{carb}$ values show a gradually decreasing trend during the first two deltaic progradations (of -1.5 ‰), coinciding with a a very gradual and small positive trend of the $\delta^{13}C_{carb}$ values. After the second progradation, $\delta^{18}O_{carb}$ rapidly returns to more positive values, maintained until the top of the section. This steadiness is not followed by the $\delta^{13}C_{carb}$ results that record a pronounced positive shift between 125 and 150 m height (of +1 ‰). At YB, the $\delta^{18}O_{carb}$ values range from -6.44o to -4.2 ‰, ((average -4.9 ± 0.4 ‰), and the $\delta^{13}C_{carb}$ values from -1.8 to 0.6 ‰ (-0.8 ± 0.4 ‰) (Fig. 7). Small oscillations (±0.5 ‰) of the $\delta^{18}O_{carb}$ dominate the lower part of the section, and ends with a significant negative shift at 285 m. There, the $\delta^{13}C_{carb}$ values decrease by 0.8 ‰ and the $\delta^{18}O_{carb}$ values decrease by 1.3 ‰. This level is organicOM rich (1.0–1.5 wt.% TOC) and shows also also a decrease of 2‰ in the $\delta^{13}C_{org}$ values (see below). Above the organic OM rich interval, the $\delta^{13}C_{carb}$ and $\delta^{18}O_{carb}$ values return to pre-event background values, with a shift to higher values towards the base of the Sabiñánigo sandstone, where the $\delta^{13}C_{carb}$ values reach the maximum value of 0.6 ‰. A gradual decrease of the $\delta^{18}O_{carb}$ values coincide coincides with the recurrent progradation events evidenced by the Sabiñánigo sandstone. In contrast, the

$\delta^{13}C_{carb}$ follows a stable trend around -1 ‰ until the top of the section. Above the Sabiñánigo sandstone and within the Pamplona marls, the $\delta^{18}O_{carb}$ values show no variance until the top of the section.

4.43.3 4 Organic carbon isotopes

At BS section, the $\delta^{13}C_{org}$ values range from -26.33‰ to -22.6 ‰ (-24.6 ± 0.5 ‰; Fig 6), including two groups of samples with different $\delta^{13}C_{org}$ values. In the first group, formed by the samples before the first siliciclastic progradation (0–50 m), the having relatively low TOC content is low (0.1–0.3 wt.%) and relatively highthe $\delta^{13}C_{org}$ valuess relatively higher (-25 to -24 ‰). The second group is formed by samples between the deltaic propagations (65–85 m), which have higher TOC content (0.3–0.5 wt.%) and lower $\delta^{13}C_{org}$ values (~ -26 ‰). At YB, the $\delta^{13}C_{org}$ values vary between -27.2 and -23.7 ‰ (-24.9 ± 0.8 ‰; Fig 6), whose lowest value of -27.2 ‰ was measured within the OM rich level at 285 m. The $\delta^{13}C_{org}$ values increase upwards till the base of the Sabiñánigo sandstone, where they show a negative spike, coinciding with the positive shift of the $\delta^{13}C_{carb}$ and $\delta^{18}O_{carb}$ values. Then the $\delta^{13}C_{org}$ values first return to the pre-event background values, and and then show a negative excursion of to 2‰ in the last two samples of the Sabiñánigo sandstone.

5 Discussion

5.1 Primary versus diagenetic signals

Chemostratigraphy arises a multitude of possible influences from differences in biological, diagenetic, and physico-chemical factors that can mask the primary signal (Wendler, 2013). To better discern primary versus altered signals, it is necessary to understand the factors controlling the primary isotopic composition and assess the potential extent of diagenetic overprint. Oxygen isotopes in carbonates are controlled by the temperature of formation, the $\delta^{18}O$ value of the carbonate-precipitating fluid ($\delta^{18}O_w$), the mineralogy (*e.g.*, higher $\delta^{18}O_{dolomite}$), and any kinetic effect manifested during the precipitation (*e.g.*, pH, salinity; Swart 2015). $\delta^{18}O$ is generally used as a temperature proxy in the marine realm, even though it is more prone to alteration (Fio *et al*. 2010). In contrast, carbon isotopes are not thought to be directly influenced by temperature and are generally more resistant to diagenetic processes (Schrag *et al*., 1995; Swart, 2015). However, $\delta^{13}C$ values are also controlled by kinetic effects, mineralogy, and mostly by the $\delta^{13}C$ trace from the dissolved organic carbon (DIC; Wendler, 2013). The isotopic signal from the DIC indicates the source of this carbon, especially the type of oxidized/respired organic matter components (Swart, 2015). In proximal depositional environments, however, this could be modified by (1) organic matter productivity and burial rate, (2) extrabasinal carbonate input, (3) water circulation/stratification and evaporation, (4) terrestrial runoff and weathering (Saltzman et al., 2012, Läuchli et al., 2021). Considering this, $\delta^{13}C$ is usually used as a global correlation tool since it can register eustatic sea-level fluctuations, changes in weathering flux, or significant perturbations in the global carbon cycle (*e.g.*, volcanic CO_2 input; Wendler 2013 and references therein).

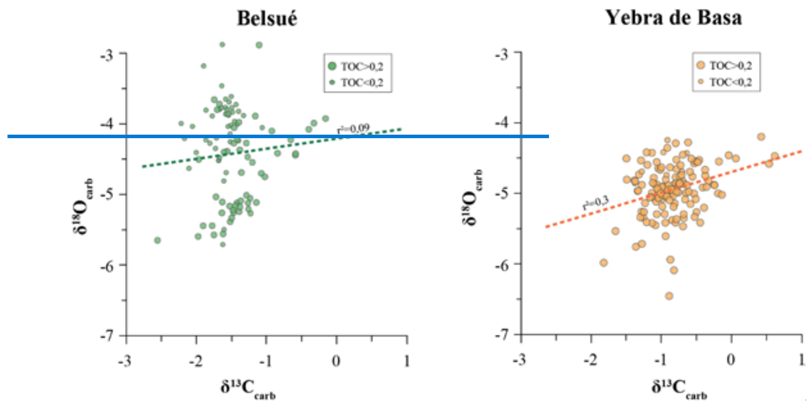

Figure 9: $\delta^{18}O_{carb}$ – $\delta^{13}C_{carb}$ scatterplot of all Belsué and Yebra de Basa samples. The regression lines are given for reference with the square correlation coefficients (r^2). The size of the symbols is small for samples with TOC < 0.2 wt.% and big for samples with TOC > 0.2 wt.%.

During carbonate diagenesis, the cementation, dissolution and re-precipitation (neo-formation), due to the interaction with post-depositional fluids —probably depleted in $\delta^{18}O$ or at higher temperature, or both— can alter the primary oxygen isotope composition (Schrag et al., 1995; Marshall, 1992). The carbon isotope composition can be also modified by differences in the contribution of biomass (marine *vs.* terrestrial), of carbonates (*e.g.* allochthonous clasts), and/or ^{13}C-depleted DIC derived from oxidation/respiration of organic matter (Marshall, 1992; Schrag et al., 1995; Wendler, 2013).

One method to assess the degree of diagenetic alteration is to evaluate the correlation between $\delta^{13}C$ and $\delta^{18}O$ values (Brasier et al., 1996). Statistically, a non-significant positive correlation ($r > 0.6$) indicates that a diagenetic overprint of the primary isotopic signature can be excluded (e.g. Fio et al. 2010). Our values from Belsué and Yebra de Basa show no significant statistical $\delta^{13}C$-$\delta^{18}O$ correlation ($r^2<0.3$) for both sections, probably suggesting non or reduced diagenetic modification of the primary signals (Fig. 9). Additionally, as proposed by Kubler and Jaboyedoff (2000), the illite crystallinity serve to assess the degree of possible alteration of the mineral assemblage by estimating the stage of diagenesis that has reached the sample. These authors compared clay mineral assemblages, illite crystallinity, and OM parameters to define four diagenetic zones. The presence of smectite within the illite-smectite (IS) mixed layers in our samples is between 20 and 30%, which according to the Kübler and Jubeyedoff (2000) zonations, fall within the 3rd diagenetic zone, i.e. shallow diagenesis (*ca.* 60 to 80ºC). Another diagenetic indicator is the maximum temperature (T_{max}) reached during the Rock-Eval Pyrolysis (S2), which marks the maturity of the organic matter. We checked T_{max} using only the samples with relatively high organic matter content (TOC>0.5wt.%; S2>0.2). The measured T_{max} values are 440ºC, corresponding to the beginning of the oil window (*ca.* 60ºC; Espitalié et al., 1985; see Fig. 8), which also agree with vitrinite reflectance and Raman measurements from this area (Labaume et al., 2016).

~~All the diagenetic evidences, among them the isotopic values correlation, the illite crystallinity, and the T_{max}, suggest that diagenetic overprint is small. Therefore, the primary isotopic signal is preserved in both sections and the geochemical results can be safely used as proxies to study paleoenvironmental conditions, and eventually be compared to global key isotopic curves during the MECO event.~~

5.1~~2~~ MECO isotopic record

In summary, at Belsué, the oxygen isotope~~ic~~ record shows a general trend towards more negative values from the base to the middle sandstone units. This trend ~~is intensified by a~~peaked with a negative $\delta^{18}O_{carb}$ shift of ~1 ‰ ~~prior to~~before the sandstone unit, just in the chron transition C19r-C18n.2n (~~Fig. 10~~Fig. 9). ~~In Yebra, the~~ The $\delta^{18}O_{carb}$ ~~oxygen isotope~~e~~ic record~~values in Yebra de Basa ~~shows~~ show a small-scale variabilit~~y~~y~~,~~ consistent with local effects~~,~~. ~~but t~~Then a negative ~~$\delta^{18}O_{carb}$~~ shift of ~1.2 ‰ occurs close ~~of the~~to the deltaic progradation (~~Fig. 10~~Fig. 9). ~~Either in Belsué or Yebra de Basa~~The ~~the~~ MECO zenith ~~(~~around the magnetic reversal C19r-C18n.2n~~;~~ (Bohaty *et al.*, 2009; Edgar *et al.*, 2010; Henehan et al., 2020) is represented by the progradation of the deltaic facies over the prodelta, ~~-~~i.e., the deltaic facies of Belsué Fm. in Belsué and the Sabiñánigo ~~sst.~~sandstones in Yebra de Basa (~~Fig. 10~~Fig. 9)~~,~~). ~~and n~~No isotopic data ~~was~~ were ~~taken in~~obtained for this interval. Nevertheless, the onset of the main thermal event, just before the sandstone occurrence, is preserved as the negative excursion. After the sandstone ~~progradation~~ progradation, ~~both Belsué and Yebra~~the $\delta^{18}O_{carb}$ ~~oxygen values~~ values in both sections return closely to those before the excursion (Fig. 9).

~~recover and become similar than before the excursion (Fig. 10~~Fig. 9)~~.~~

Con formato: Fuente: Cursiva

Con formato: Fuente: Cursiva

Con formato: Sin Resaltar

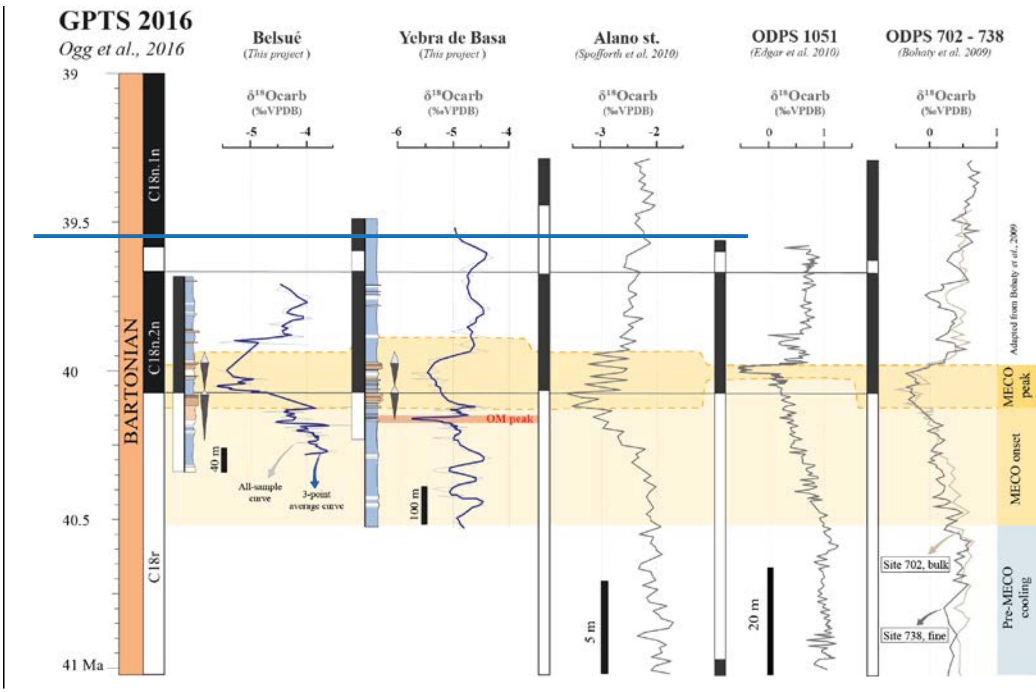

GPTS 2016
Ogg et al., 2016
Belsué
(This project)
Yebra de Basa
(This project)
Alano st.
(Spofforth et al. 2010)
ODPS 1051
(Edgar et al. 2010)
ODPS 702 - 738
(Bohaty et al. 2009)
δ18Ocarb (‰VPDB)
39
39.5
40
40.5
41 Ma
BARTONIAN
C18n.1n
C18n.2n
C18r
40 m
100 m
5 m
20 m
All-sample curve
3-point average curve
OM peak
Site 702, bulk
Site 738, fine
Adapted from Bohaty et al., 2009
MECO peak
MECO onset
Pre-MECO cooling

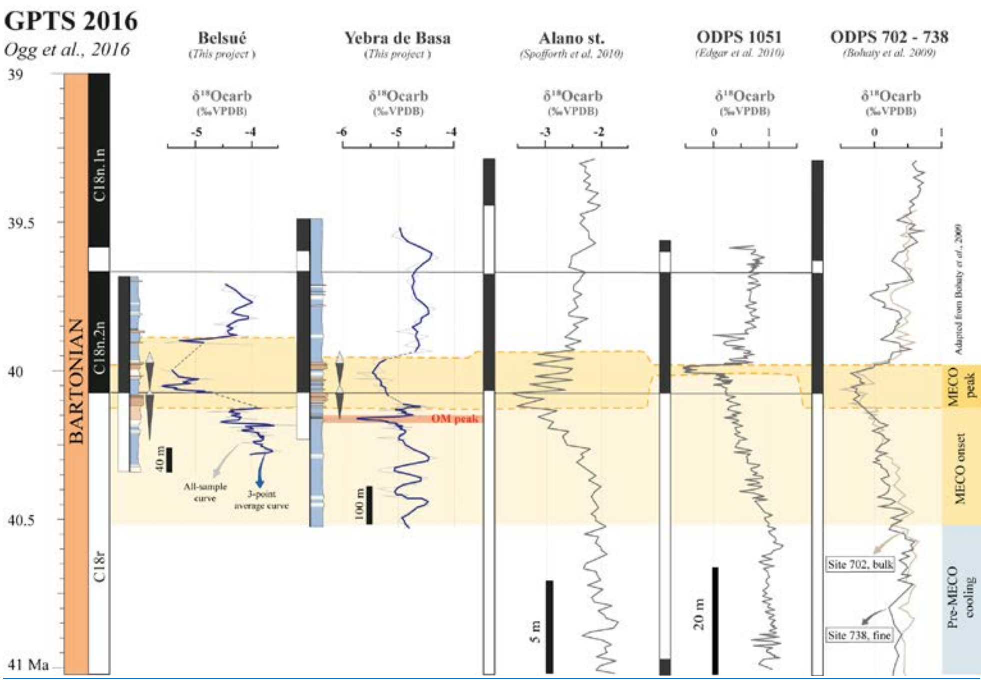

Figure 10Figure 9: Oxygen isotopeic ($\delta^{18}O_{carb}$) correlation panel for the studied sections (Belsué and Yebra de Basa) with MECO target curves from Alano (Italy, Tethys oceanTethys Ocean, Spofforth *et al.*, 2010), ODPS 1051 (N Atlantic Ocean; Edgar *et al.*, 2010), ODPS 702 (S Atlantic Ocean; Bohaty et al., 2009) and ODPS 738 (S Indic Ocean; Bohaty et al., 2009). Data from the bulk and fine sediments fractions. Highlighted in red the organic matterOM (OM peak) rich interval (TOC peak) in Yebra de Basa. The two progradation-retrogradation cycles referred in the text are drawn with grey and white triangles. The data is scaled accordingaccording to magnetostratigraphic tie points, between C18r-18n.2n and C18n.2n-C18n.1r chrons.

The trend observed in the studied sections of the South Pyrenean Basin (SPFB) SPFB is shared with most ofmost high-resolution offshore and nearshore isotopic records of the MECO (Bohaty *et al.*, 2009; Bohaty and Zachos, 2003; Edgar *et al.*, 2010, 2020; Spofforth *et al.*, 2010; Jovane *et al.*, 2007; GiorginiGiorgioni *et al.*, 2019; Galazzo *et al.*, 2014). They all that also show the same trend towards more negative $\delta^{18}O_{carb}$ $\delta^{18}O$ values, which is intensifying intensified during the MECO peak (Fig. 10Fig. 9). TheSimilarly, the end of the event is defined marked in both sections by a rapid increase in of the $\delta^{18}O_{carb}$ values of by ~1 ‰, similar toas reported in other sites sections worldwide (Bohaty *et al.*, 2009; Galazzo *et al.*, 2014; Edgar *et al.*, 2010, 2020; Giorgioni *et al.*, 2019; Spofforth *et al.*, 2010).

Contrarily to the agreement between our new data and most of the available oxygen isotopeic records, the $\delta^{13}C_{carb}$ results do not show a clear correlation with global target curvescurves (Fig. 7). On one hand, the Belsué section records a positive $\delta^{13}C_{carb}$ excursion, presenting with a delay respect the $\delta^{18}O_{carb}$ minimum,. and The Yebra de Basa section shows a prominent positive

Con formato: Fuente: Cursiva
Con formato: Fuente: Cursiva
Con formato: Fuente: Cursiva
Con formato: Fuente: Cursiva
Con formato: Fuente: Cursiva
Con formato: Fuente: Cursiva
Con formato: Fuente: Cursiva
Con formato: Fuente: Cursiva
Con formato: Fuente: Cursiva
Con formato: Fuente: Cursiva
Con formato: Fuente: Cursiva
Con formato: Fuente: Cursiva
Con formato: Fuente: Cursiva
Con formato: Fuente: Cursiva

$\delta^{13}C_{carb}$ excursion just before the main deltaic progradation (320~~-~~–340 m from YB). On the other hand, most of the oceanic geochemical records show a small ~~Carbon~~ carbon ~~Isotope~~isotope~~ic~~ ~~Excursion~~ excursion (CIE) at the MECO peak of warming (~40 Myr; Westerhold and Röhl, 2013; Bohaty *et al.*, 2009; Spofforth *et al.*, 2010), but before and after the $\delta^{13}C_{carb}$ values are ~~carbon is~~ highly variable, showing opposite trends between hemispheres (Henehan *et al.*, 2020; Giorgioni *et al.*, 2019). This CIE, like in other ~~sites in the~~ northern hemisphere sites (Sppofforth *et al.*, 2010; Giorgioni *et al.*, 2019), is not well represented in our data. Therefore, our $\delta^{13}C_{carb}$ ~~results~~ data seem to confirm ~~m the fact that~~that the MECO is not associated with ~~a large~~an extensive input of depleted ^{13}C ~~carbon in~~in ~~t~~ the ~~environment~~ environment, as suggested in a ~~previous~~ stud~~ies~~y ~~suggest~~ (Henehan *et al.*, 2020~~),~~). ~~although~~However, an alternative ~~is~~ explanation for this discrepancy would be that the sandstone progradation masked the CIE. ~~the CIE could be masked by the sandstone progradation itself.~~

Instead of a global origin, however, ~~these~~ the $\delta^{13}C_{carb}$ variations could ~~be related~~be caused by ~~with~~ local changes in the carbon isotope composition of the dissolved inorganic carbon (DIC), pH, rate, and temperature of carbonate precipitation, and its mineralogy (e.g., Swart, 2015). ~~sources or changes in the mineralogy (*e.g.*, dolomite).~~ Here, given the proximity of the continent in the shelf environment of the studies section, we cannot rule out that spatial and temporal variation in freshwater input of different components (i.e., ~~that fresh water~~ riverine/estuarine and groundwater sources) ~~(and groundwater) input fluctuations~~

could have altered the ~~carbon~~ isotopic composition of the DIC and the carbonate $\delta^{13}C$ and $\delta^{18}O$ values (e.g., Marshall, 1992; Saltzman and Thomas ~~et al.,~~, 2012; Wendler, 2013 Läuchli *et al.*, 2021)~~, representing the terrestrial contribution to the oceanic carbon reservoir.~~ This ~~contribution should've~~freshwater input could produce carbonate depleted in ^{13}C and ^{18}O (see detailed discussion in section 5.2). ~~shifted towards more negative values the entirety of the signal, affecting both carbon and oxygen isotopes.~~ The fact that ~~our results~~the Belsué and Yebra de Basa isotopic records preserve the MECO excursion in $\delta^{18}O_{carb}$~~,~~ ~~tells us that~~suggests that the $\delta^{13}C_{carb}$ values could also ~~composition should also~~ record ~~the~~a global signal~~,~~. However, ~~although~~ this is difficult to ~~assess~~appreciate because of the small $\delta^{13}C_{carb}$ variations in the studied sections and the somewhat variable and peculiar published ~~given the weakness and variability of the $\delta^{13}C_{carb}$ MECO signal. Th~~~~Thus, given the observed~~~~our small $\delta^{13}C_{carb}$ variations and the rather variable and peculiarpeculiar~~ carbon isotope~~ic~~ record during the MECO~~,~~. Therefore, the correlations were ~~focus our correlation~~based on the $\delta^{18}O_{carb}$ records (Fig. 9). In summary, our results record a decoupling between oxygen and carbon isotopes. The $\delta^{18}O_{carb}$ values seem to follow the global trend, while the variation of the $\delta^{13}C_{carb}$ values remains ambiguous. The particular carbon isotope record during the MECO, with variable and opposite trends between hemispheres (Henehan *et al.*, 2020), and a brief negative carbon isotope excursion recorded just at some sites (Westerhold and Röhl, 2013; Bohaty *et al.*, 2009; Spofforth *et al.*, 2010), could be an explanation. However, given the location of the studied sections on a continental shelf, it is important to check the possible diagenetic influence or alteration of the primary isotopic signal.

Con formato: Fuente: Cursiva
Con formato: Fuente: Cursiva
Con formato: Fuente: Cursiva
Con formato: Fuente: Cursiva
Con formato: Fuente: Cursiva
Con formato: Fuente: Cursiva
Con formato: Fuente: Cursiva
Con formato: Superíndice
Con formato: Superíndice
Con formato: Inglés (Estados Unidos)
Con formato: Fuente: Cursiva
Con formato: Superíndice
Con formato: Superíndice
Con formato: Fuente: Cursiva
Con formato: Fuente: Cursiva
Con formato: Fuente: Cursiva
Con formato: Subíndice

5.2 Primary versus diagenetic signals

~~**Our isotopic results record a decoupling between oxygen and carbon, where $\delta^{18}O_{carb}$ seem to follow the global trend while $\delta^{13}C_{carb}$ remains ambiguous. The particular carbon isotope record during the MECO, with variable and opposite trends between hemispheres (Henehan et al., 2020), and a brief negative carbon isotope excursion (NCIE) recorded just at some sites (Westerhold and Röhl, 2013; Bohaty et al., 2009; Spofforth et al., 2010), could be an examplanation. However, given the location in a continental shelf, we wanted to check the possible diagenetic influence or alteration of the primary signal.**~~

The carbonate primary carbon and oxygen isotope compositions may be affected by postdepositional processes, including the neoformation of authigenic and diagenetic phases. Therefore, before the paleoenvironmental interpretation of $\delta^{13}C_{carb}$ and $\delta^{18}O_{carb}$ records from shallow marine environments, it is necessary to determine primary versus diagenetic signal components. This discrimination requires understanding the factors controlling the primary marine isotopic composition and an evaluation of potential diagenetic overprints on the original geochemical signatures (e.g., Marshall, 1992; Schrag *et al*., 1995). ~~Chemostratigraphy arises a multitude of possible influences from differences in biological, diagenetic, and physico-chemical factors that can mask the primary signal (Wendler, 2013; Marshall. 1992). To better discern primary versus altered signals, it is necessary to understand the factors controlling the primary isotopic composition and assess the potential extent of diagenetic overprint.~~ Oxygen isotopes in carbonates are controlled by the temperature of formation, the $\delta^{18}O$ value of the carbonate-precipitating fluid ($\delta^{18}O_w$), the mineralogy (*e.g.*, higher $\delta^{18}O$ in dolomite vs. calcite~~dolomite~~), and any environmental parameter (e.g., pH, salinity) affecting the ~~kinetic effect manifested during th~~rate ~~e~~of carbonate precipitation (~~*e.g.*, pH, salinity;~~ Swart, 2015). The effect of diagenetic alteration is more pronounced in the case of oxygen isotopes than carbon isotopes due to the high amount of oxygen relative to carbon present in postdepositional fluids and their variable $\delta^{18}O$ values (e.g., Marshall, 1992; Schrag *et al*., 1995; Fio *et al*., 2010). ~~$\delta^{18}O$ is generally used as a temperature proxy in the marine realm, even though it is usually more prone to alteration (Fio *et al*. 2010).~~ Carbonate with low $\delta^{18}O$ values can be produced by increasing temperature, freshwater input, and meteoric diagenesis, whereas ^{18}O enrichment could indicate either lower temperature or evaporation (e.g., Marshall, 1992; Patterson and Walter,1994; Schrag et al., 1995). In contrast, carbon isotopes are not thought to be directly influenced by temperature and are generally more resistant to diagenetic processes (Patterson and Walter,1994; Schrag *et al*., 1995; Swart, 2015). However, $\delta^{13}C$ values are also controlled by kinetic effects, mineralogy, and ~~mostly~~mainly by the $\delta^{13}C$ ~~trace~~value from the ~~dissolved organic carbon~~DIC (~~DIC;~~ Wendler, 2013). The primary diagenetic process that affects the $\delta^{13}C$ values of the DIC is the oxidation of the organic matter, which produce CO_2 (and DIC species) depleted in ^{13}C (low $\delta^{13}C$ values). Therefore, the $\delta^{13}C$ values of the DIC and derived carbonates ~~The isotopic signal from the DIC~~ indicat~~e~~se the source ~~of this~~of carbon~~ carbon~~, ~~especially~~including the type of degraded/oxidized~~/respired~~ ~~organic matte~~organic matter (OM) of different types,~~r components~~ original seawater carbon, skeletal and non-skeletal carbonate sources (e.g., Swart, 2015). In proximal depositional environments, however, the $\delta^{13}C$ values ~~this~~ could be modified by (1) ~~organic matter~~OM source, productivity, and burial rate, (2) extrabasinal carbonate input, (3) water circulation/stratification and evaporation, (4) terrestrial runoff and weathering (Saltzman ~~et al~~and Thomas~~.~~, 2012, Läuchli *et al*., 2021). Considering this, $\delta^{13}C$ is usually used as a

Con formato: Título 2
Con formato: Sin Resaltar
Con formato: Fuente: Cursiva
Con formato: Fuente: Cursiva
Con formato: Fuente: Cursiva
Con formato: Fuente: Cursiva
Con formato: Inglés (Estados Unidos)
Con formato: Fuente: Cursiva
Con formato: Inglés (Estados Unidos)
Con formato: Inglés (Estados Unidos)
Con formato: Inglés (Estados Unidos)
Con formato: Inglés (Estados Unidos)
Con formato: Inglés (Estados Unidos)
Con formato: Inglés (Estados Unidos)
Con formato: Inglés (Estados Unidos)
Con formato: Inglés (Estados Unidos)
Con formato: Fuente: Cursiva

global correlation tool since it can register eustatic sea-level fluctuations, changes in weathering flux, or significant perturbations in the global carbon cycle (*e.g.*, volcanic CO_2 input; Wendler 2013 and references therein).

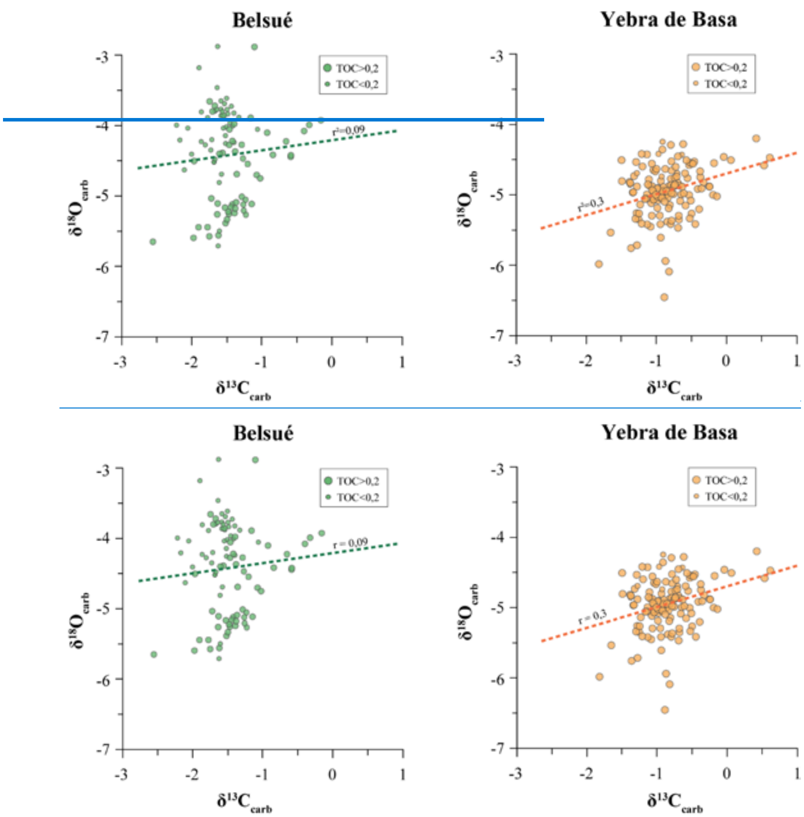

Figure 10: $\delta^{18}O_{carb}$ - $\delta^{13}C_{carb}$ scatterplot of all Belsué and Yebra de Basa samples. ~~The regression lines are given for reference with the square correlation coefficients (r²Pearson correlation coefficient (r).~~ The size of the symbols is small for samples with TOC < 0.2 wt.% and big for samples with TOC > 0.2 wt.%. The Pearson correlation coefficients (r) and regression lines are shown.

~~To assess t~~The degree of diagenetic alteration ~~we used~~was assessed through three different ~~methods~~approaches. First, was evaluated the ~~correlation~~relationship between $\delta^{13}C$ and $\delta^{18}O$ values (Brasier *et al.*, 1996). Statistically, a non-significant correlation (Pearson correlation coefficient; *r* < 0.6) indicates that a diagenetic overprint of the primary isotopic signature can be excluded (e.g., Fio *et al.*, 2010). ~~Our values from Belsué and Yebra de Basa show n~~In both sections, no ~~significant~~ statistical significant correlation (*r* < 0.3) was found between the $\delta^{13\,8}$~~C~~O_{carb} and $\delta^{18\,3}$~~O~~C_{carb} ~~correlation~~values ~~(*r* < 0.3) for both sections,~~.

Con formato: Fuente: Cursiva

Con formato: Fuente: Cursiva

Con formato: Fuente: Cursiva

Con formato: Subíndice

This lack of relationship -suggests that ~~probably suggesting non or reduced~~no or minor diagenetic ~~modificati~~modifications affected~~on of~~ the primary isotopic ~~signals~~compositions (Fig. ~~.~~10). The second approach used to assess the degree of alteration uses clay mineralogy. Kübler~~Additionally, as proposed by Kubler~~ and Jaboyedoff (2000~~), the illite crystallinity serve to assess the degree of possible alteration of the mineral assemblage by estimating the stage of diagenesis that has reached the sample. These authors~~) defined four diagenetic zones by compar~~ed~~ing ~~clay mineral assemblages,~~ illite crystallinity~~,~~ -with mineral assemblages and ~~OM parameters~~organic matter type~~ to define four diagenetic zones~~. ~~The presence of smectite within the illite-smectite (IS) mixed layers in our samples~~The Belsué and Yebra de Basa samples have 20–30% smectite within the illite-smectite (IS) mixed layers and are within the 3rd diagenetic zone of Kübler and J~~au~~beyedoff (2000), -i.e., shallow diagenesis (*ca.* 60~~ to~~ –80ºC~~)~~). ~~is between 20 and 30%, which according to the Kübler and Jubeyedoff (2000) zonations, fall within the 3rd diagenetic zone, i.e. shallow diagenesis (ca. 60 to 80ºC).~~ Another diagenetic indicator is the maximum temperature (T_{max}) reached during the Rock-Eval Pyrolysis (S2), which marks the maturity of the ~~organic matter~~OM. ~~We checked T_{max} using only the samples with relatively high organic matter content (TOC>0.5wt.%; S2>0.2).~~ The ~~measured~~ T_{max} –values obtained in samples with relatively high OM content (~~(~~TOC ≥ 0.5 wt.%; S2 ≥ 0.2~~).~~) ~~a~~were < 440ºC (Fig. 8), ~~corresponding~~which corresponds to the beginning of the oil window (*ca.* 60ºC; Espitalié et al., 1985~~; see Fig. 8)~~. ~~which also~~This maturity level of the organic matter agrees with vitrinite reflectance and Raman measurements ~~from this area~~in the studied area (Labaume et al., 2016). In summary, the three approaches for assessment of the diagenetic degree, i.e., carbonate $\delta^{13}C$ and $\delta^{18}O$ values, illite crystallinity, and thermal maturation of the organic matter (T_{max}),

~~All the diagenetic evidences, among them the isotopic values correlation, the illite crystallinity, and the T_{max},~~ suggest that the diagenetic overprint in the studied Belsué and Yebra de Basa rocks is ~~small~~low. The ~~Therefore, the~~ primary isotopic signal is preserved largely in both sections~~.and~~ It ~~the geochemical results~~ can be safely use~~d~~d ~~as proxies~~ to study paleoenvironmental conditions~~,~~ and ~~eventually~~ be compared to global key isotopic curves during the MECO event.

5.3 The organic matter peak in Yebra de Basa

In Yebra de Basa (YB) section, an increase in ~~organic matter~~TOC content at the 280–290 m interval (up to 1.5 wt.% TOC) is associated with a negative isotope excursion of -1.5‰ for $\delta^{18}O_{carb}$, -2.0‰ for $\delta^{13}C_{org}$ and -0.8‰ for $\delta^{13}C_{carb}$ values (Fig. 7 and 9). The ~~OM~~ OM-rich interval occurs 50 ~~meters~~ m below the main Sabiñánigo sandstone progradation in Yebra de Basa~~, and i~~. It is not coincident with the ~~main~~ prominent increase of detrital input, marked by an increase in grain size. This boost ~~in organic matter~~in OM burial is also observed in the Neo-Tethys region, like in Italy (Spofforth *et al.*, 2010) and the Crimea-Caucasus (Benyamovsky *et al.*, 2012), which may ~~had~~ have played an important role in carbon drawdown and rapid cooling after the MECO event (Bohaty *et al.*, 2009, Henehan *et al.*, 2020).

Several possibilities could explain the presence of an OM-rich interval before a deltaic progradation. First, a significant freshwater input in a restricted basin can lead to water stratification where anoxic conditions are ~~favoured~~favoured, ~~this resulting in an increase of~~increasing OM preservation~~,~~ independently of its source. Nevertheless, the slight increase in redox-

Con formato: Sin Resaltar

Con formato: Fuente: Cursiva

Con formato: Fuente: Cursiva

Con formato: Fuente: Cursiva

Con formato: Fuente: Cursiva

sensitive elements (V and Mo, Fig. 6) is too limited to support the development of water stratification and the resulting suboxic-anoxic conditions (Tribovillard *et al.*, 2006). Second, the enhanced freshwater input could have increased nutrient availability ~~and the consequent~~and marine productivity. We, however, reject this hypothesis because ~~our~~ the geochemical data~~organic matter analyses~~ ~~show~~ point to main ~~a clear~~ terrestrial ~~compound~~ components of the organic matter (low HI-OI) and no ~~sign of~~low nutrient availability increase (low Ni concentration; Tribovillard et al., 2006). ~~Our~~ Therefore, the most probable ~~preferred~~ explanation is that the OM peak could be related to a significant increase in detrital input and terrestrial OM. The presence of several dark-marl beds westwards suggests it was not a unique episode~~,~~ but ~~instead~~ a series of recurrent events (Boya, 2018). In addition, the terrestrial origin is also supported by the strong correlation (r ~~>~~> 0~~,~~.7) observed between the siliciclastic elements (Al, Ti, Fe~~$^{3+}$~~) and the TOC or all the OM-related trace elements (V, Mo, Ba, and Th; Tribovillard *et al.*, 2006). Despite this, the isotopic results do not agree with this correlation~~,~~ because pre-Miocene marine OM had lower $\delta^{13}C$ than terrestrial OM (Popp *et al.*, 1989). Thus, an alternative explanation for the negative $\delta^{13}C_{org}$ and $\delta^{13}C_{carb}$ excursion may be an increased input of organic matter released from soils containing bacterial biomass with low $\delta^{13}C_{org}$ values (Fio *et al.*, 2010). ~~This~~ This agrees with the Rock-Eval ~~is in agreement with our Rock evaluation and geochemical results~~results, ~~that~~ which point towards a terrestrial origin for this organic matter (Fig. 8).

As a result, the Sabiñánigo sandstone represents a singular deltaic event embedded in ~~long~~ long-lasting prodelta conditions (Vinyoles et al., 2021) in which no evident organic events occur. Therefore, we interpret the occurrence of the ~~OM~~ OM-rich level just before the Sabiñánigo sandstone as ~~a~~ the first indicator of a shift towards a setting with more fluvial conditions, being the first evidence of the main MECO excursion in the region.

5.4 MECO response in the South Pyrenean Foreland Basin

The integration of available age constraints (Garcés *et al.*, 2014; Vinyoles *et al.*, 2021) and the new high-resolution isotopic record show that MECO's warming peak (~ 40 Ma) is associated with isochronous progradation, which can be followed all along the SPFB source-to-sink system (Fig. 11; Vinyoles *et al.*, 2021). In ~~the The~~the Tremp-Graus ~~basin~~ Basin, the Escanilla fluvial system was fed by the Sis-Gurp and Pobla alluvial systems, where a grain size increase is recorded at *ca.* 40 Ma (Whittaker *et al.*, 2011). Downstream, in the time-equivalent sections in the Ainsa basin, an anomalous amalgamated Olsón sheet stands out from the landscape as a continuous and thick conglomeratic bed, interpreted as a stacking of several braided river channels (Fig. 11; Verité, 2019; Labourdette *et al.*, 2011; Puigdefàbregas, 1975; Vinyoles *et al.*, 2021). In the deltaic counterparts (Jaca basin), a significant progradation of deltaic deposits on top of slope marls is observed in ~~our~~ the studied sections (BS and YB; Lafont, 1994; Puigdefabregas *et al.*, 1975, Vinyoles *et al.*, 2021). Finally, in the deeper sink environments of the Jaca and Pamplona basins, the correlation with the turbiditic systems is still debated and needs further research. Previous works (Puigdefàbregas, 1975; Lafont, 1994) interpreted these deltaic sequences as eustatic fluctuations of the relative sea level, which can relate to different possibilities, such as thermal expansion or glacioeustasy. Ephemeral ice sheets in Antarctica during the Middle Eocene are likely, and it seems plausible that the progressive shift towards icehouse conditions could have significant implications during the MECO (Edgar et al., 2007; Huyghe *et al.*, 2012; Baatsen *et al.*, 2020). However,

Con formato: Fuente: Cursiva
Con formato: Fuente: Cursiva
Con formato: Fuente: Cursiva
Con formato: Fuente: Cursiva
Con formato: Sin Resaltar
Con formato: Fuente: Cursiva
Con formato: Fuente: Cursiva
Con formato: Fuente: Cursiva
Con formato: Fuente: Cursiva
Con formato: Fuente: Cursiva
Con formato: Fuente: Cursiva
Con formato: Fuente: Cursiva
Con formato: Fuente: Cursiva
Con formato: Fuente: Cursiva
Con formato: Fuente: Cursiva

considering the temperature increase interpreted during the MECO zenith (+4 to 6ºC; Bohaty *et al.*, 2009), we should expect a sea-level rise (ice caps melting and thermal expansion) instead of the observed regression and system progradation. Alternatively, an abrupt ~~increase in~~ sediment supply increase can also explain a progradation of deltaic systems. Several studies observed that the main Paleogene hyperthermals are often associated with an enhanced flux of terrigenous material interpreted as a boost of the hydrological cycle and higher seasonality (Schmitz *et al.*, 2001; Chen *et al.*, 2018; Foreman *et al.*, 2017; Pujalte *et al.*, 2015). Although the MECO is not an abrupt event like other hyperthermals~~, ,but~~ instead a more extended period of gradual warming (*ca.* 500 kyr; Bohaty *et al.*, 2009), we also observe this progradation focused during the warming peak (*ca.* 40 Ma). Accordingly, an explanation for the progradation is that the MECO prolonged warming produced an enhanced hydrological cycle that ~~favoured~~favoured sediment production and transport, thus leading to an increase in sediment supply and ~~favouring~~favouring the system progradation at the peak of the event. The nature of a greater sediment provision (Qs) should be originated upstream, for instance, linked to enhanced sediment remobilization (e.g., floodplain) or accelerated hillslope processes (Foreman *et al.*, 2012).

Con formato: Fuente: Cursiva

Con formato: Fuente: Cursiva

Con formato: Fuente: Cursiva

Con formato: Fuente: Cursiva

Con formato: Fuente: Cursiva

Con formato: Fuente: Cursiva

Con formato: Fuente: Cursiva

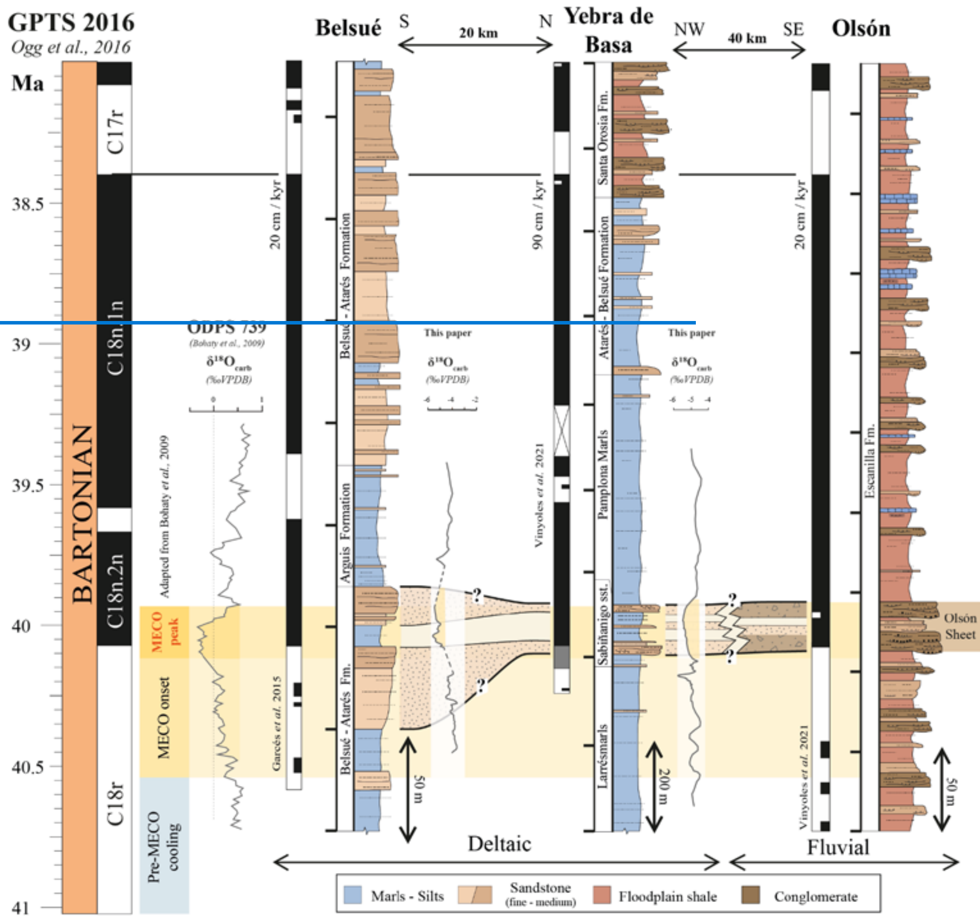

Con formato: Centrado

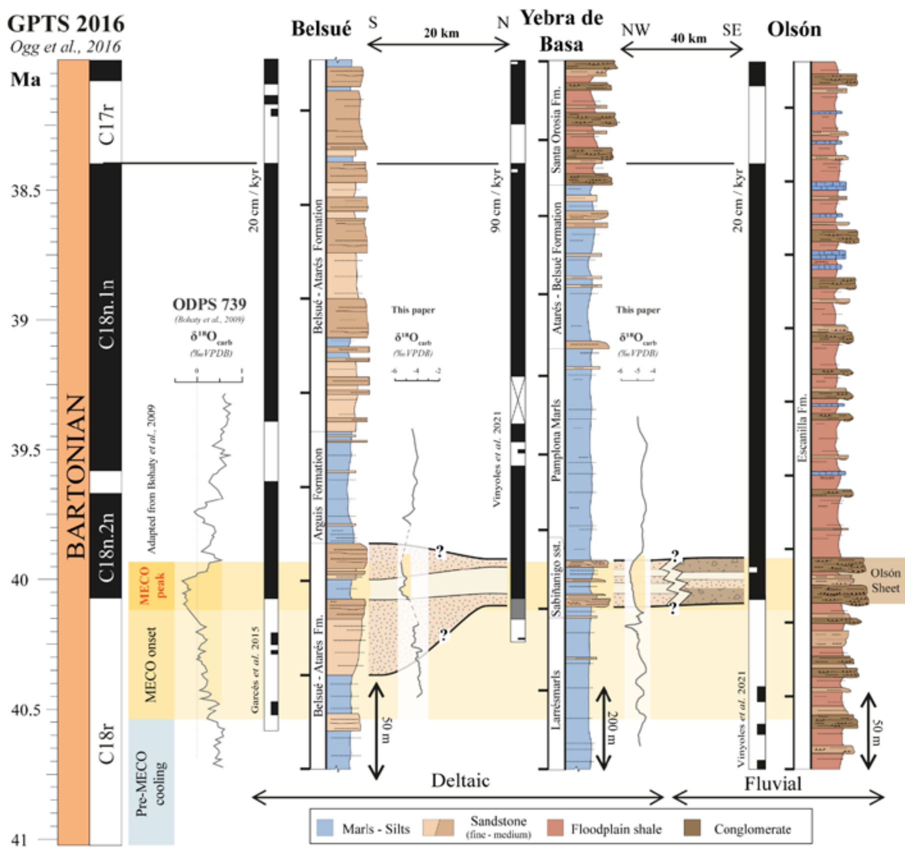

Figure 11: Correlation panel between Belsué, Yebra de Basa, and Olsón section with the GPTS 2016 (Ogg et al., 2016). The stratigraphic sections are modified from Garcés *et al.* (2014) and Vinyoles *et al.* (2020). The oxygen isotopic ~~record~~ (δ $^{18}O_{carb}$) record from ODPS 738 and the MECO age constraints defined by yellow and blue bars are modified from Bohaty et al. (2009). The oxygen isotopic record (δ $^{18}O_{carb}$) from Belsué and Yebra de Basa correspond to our results, and the dashed lines represent non-sample intervals. The sedimentation rate (SR) from Belsué, Yebra de Basa, and Olsón, are average SR between chron C18n.2n and C17r, from Vinyoles *et al.*, 2021 data.

Therefore, the coincidence in time of a basin-wide progradation in the SPFB and the MECO might implicate~~might implicate~~ a link between them. Our geochemistry analyses also suggest a terrestrial origin for this OM, which point towards an increase in soil remobilization, ~~erosion~~erosion, and transport in continental environments during the MECO event.

Con formato: Fuente: Cursiva

Con formato: Fuente: Cursiva

Con formato: Fuente: Cursiva

5.5 Global implications and correlation

The global impact of the MECO event in continental settings remains ~~currently~~ poorly documented, with only a few studies in continental environments performed around the globe (e.g., Bosboom *et al*., 2014; Mulch *et al*., 2015). In the North American plateau, a boost of precipitation during the MECO is derived from lower $\delta^{18}O_{carb}$ values (Mulch *et al*., 2015). In contrast, in the Tarim basin (China), a shift towards arid conditions has been interpreted from a reduction in fern palynomorphs (Bosboom *et al*., 2014). This aridification trend in central Asia differs from the documented Neo-Tethys O~~o~~cean dynamic, where marine records show an increase in organic matter (OM) burial during the MECO peak and part of the post-MECO recovery (Spofforth *et al*., 2010; Giorgioni *et al*., 2019 Benyamovskiy *et al*., 2012). Increased sediment supply due to enhanced erosion and transport ~~clearly pp~~provides a mechanism for the more efficient burial of OM during this and other hyperthermals (Galy et al., 2007). If this enhanced OM burial is global or sufficiently widespread (it is absent in several sections, including Belsué in this study), it could represent an important mechanism to explain the carbonate $\delta^{13}C$ increase that is recorded globally during the post-event recovery and the associated rapid return to pre-event conditions, maybe playing an essential role in the drawdown of atmospheric carbon (e.g., Bohaty *et al*., 2009; Henehan *et al*., 2020; Sluijs *et al*., 2013; Edgar *et al*., 2020; Giorgioni *et al*., 2019; Spofforth *et al*., 2010).

Considering the long duration of the MECO event (*ca.* 500 kyr; Bohaty *et al*., 2009), some of the most important effects in the ocean occur during its peak phase, *e.g.*, ocean acidification (Bohaty *et al*., 2009; Henehan *et al*., 2020; Arimoto *et al*., 2020) or OM burial (Giorgioni *et al*., 2019; Spofforth *et al*., 2010). In the SPFB, the continental progradation also occurred at the end of the event, supported by the sedimentological and geochemical ~~evidences~~evidence that shows an increase of sediments delivered to the sea, including large amounts of organic matter of terrestrial origin. Hence, our work suggests a link between enhanced hydrological cycles and enhanced OM transport and burial, ~~which~~ possibly ~~account~~ accounting for the observations of enhanced OM burial around the Neo-Tethys region. This response in sediment delivery rate, OM burial in shallow and restricted basins, ~~as well as ocean acidification,~~ has been previously documented for other early Eocene hyperthermals (Chen *et al*., 2018; Foreman *et al*., 2012, 2014; Pujalte *et al*., 2015; Foreman and Straub, 2017; Honegger *et al*., 2020). Hence, ~~the MECO,~~ despite its important differences with the early Eocene hyperthermals, ~~yet~~ the MECO shares several attributes with them around the warming peak. In summary, our results point to a more intense hydrological cycle perturbing rainfall patterns in the Pyrenean region during the MECO peak~~,~~ and leading to increased sediment supply, expressed by a major progradation of sedimentary systems and, eventually, an increase in OM burial in the nearby oceanic basins.

6. Conclusions

In the South-Pyrenean Foreland Basin, an important progradation affected the entire sediment routing system from fluvial to deltaic environments at times of the Middle Eocene Climatic Optimum MECO. Here we present a new high-resolution multiproxy dataset, including stable isotopes, Rock-Eval, XRF, and clay minerals, covering the different MECO phases from two ~~well~~ well-dated key sections. The new stable isotopes records from Belsué (BS) and Yebra de Basa (YB) sections show a significant negative shift in the shallow marine sediments, around the main warming peak of the MECO event, for the first time reported in the Pyrenean region. In Yebra de Basa, an organic-rich interval of terrestrial origin is found before the main deltaic progradation~~,~~. ~~and i~~It is associated with a negative excursion in oxygen and carbon isotopes. The correlation between ~~of~~ the MECO~~,~~ and the basin-wide progradation, and ~~our~~ the new geochemical results ~~presents~~ present compelling evidence for a climatic driver, suggesting an enhanced hydrological cycle in the Pyrenean region that caused a boost in sediment and carbon export. This is in agreement with previous studies from the ~~Neo-Tethys ocean~~Neo-Tethys Ocean that recorded an increase in organic matter burial during the peak of the MECO and early post-MECO.

Although the duration of the MECO and its isotopic signature differ with respect to early Eocene hyperthermals (e.g., PETM), there are similarities around the warming peak that trigger a comparable response, including ocean acidification, ~~OM~~ organic matter burial, or a boost in sediment supply export from land to sea. Nevertheless, further work is needed to understand the role of potential sediment supply increase from the proximal continental environments towards the deeper oceanic basins, and importantly, quantify sediment and organic export, and its ~~relation~~relationship with carbon burial and silicate weathering.

Our results support the view that high-accommodation settings in foreland basins are important recorders of paleoenvironmental signals, even in shallow marine environments. Although certainly noisy, the fact that climate signals are preserved in these settings provides a range of potentially expanded sections that can be an interesting complement to high-resolution but more condensed deep-sea paleoclimatic records. In particular, during high-CO_2 globally warm episodes of the Earth's history when the carbonate-rich oceanic records may undergo intervals of non-deposition or dissolution.

Data availability

All the data (stable isotopes, clay minerals, organic matter, major and trace elements) can be found in the supplementary material.

Authors contribution

SPC led fieldwork, sampling, sample preparation, data interpretation, and writing. LV contributed to the fieldwork, data interpretation, discussion, and writing. JES performed stable isotope analyses, data interpretation, discussion, and writing. TA performed XRD analyses, data interpretation, and discussion. JV and AV contributed to the field work preparation, ~~sampling~~sampling, and discussion. MT, SW and NS contributed to the discussion, and writing. CP contributed to fieldwork, discussion, and writing. AV and MG helped with magnetostratigraphic data interpretation and discussion. SC supervised the project, funding, ~~interpretation~~interpretation, and writing.

Competing interest

The authors declare that they have no competing interests.

Acknowledgments

The authors would like to acknowledge the *Societé de Physique et d'Histoire naturelle de Genève* and Equinor (grant to Castelltort) for financing part of the field missions. We also acknowledge Marta Roigé and Salvador Boya for their help during field campaigns and the long scientific discussions. We finally acknowledge Antoine de Haller from *Université de Genève* for his help during XRF analyses.

References

Adatte, T.: Lithostratigraphic and mineralogic correlations of near K/T boundary clastic sediments in northeastern Mexico: Implications for origin and nature of deposition, Special Paper 307: The Cretaceous-Tertiary Event and Other Catastrophes in Earth History, Volume 307, 211–226, doi:10.1130/0-8137-2307-8.211, 1996.

Adatte, T., Bolle, M. P., Kaenel, E. D., Gawenda, P., Winkler, W., and Von Salis, K.: Climatic evolution from Paleocene to earliest Eocene inferred from clay-minerals: A transect from northern Spain (Zumaya) to southern (Spain, Tunisia) and southeastern Tethys margins (Israel, Negev), GFF, 122 (1), 7-8, https://doi.org/10.1080/11035890001221007, 2000.

Arimoto, J., Nishi, H., Kuroyanagi, A., Takashima, R., Matsui, H., and Ikehara, M.: Changes in upper ocean hydrography and productivity across the Middle Eocene Climatic Optimum: Local insights and global implications from the Northwest Atlantic. Global and Planetary Change, 193, https://doi.org/10.1016/j.gloplacha.2020.103258, 2020.

Baatsen, M., Von Der Heydt, A. S., Huber, M., Kliphuis, M. A., Bijl, P. K., Sluijs, A., and Dijkstra, H. A.: The middle to late Eocene greenhouse climate modelled using the CESM 1.0. 5. Climate of the Past, 16(6), https://doi.org/10.5194/cp-16-2573-2020, 2020.

Beamud, E., Garcés, M., Cabrera, L., Muñoz, J. A., and Almar, Y.: A new middle to late Eocene continental chronostratigraphy from NE Spain. Earth and Planetary Science Letters, 216(4), 501-514, https://doi.org/10.1016/S0012-821X(03)00539-9, 2003.

Behar, F., Beaumont, V., and Penteado, H. D. B.: Rock-Eval 6 technology: performances and developments. Oil and Gas Science and Technology, 56(2), 111-134, https://doi.org/10.2516/ogst:2001013, 2001.

Benyamovskiy V.N. A high resolution Lutetian–Bartonian planktonic foraminiferal zonation in the Cremean– Caucasus region of the Northeastern Peri-Tethys, Austrian Journal of Earth Science, V. 105/1. P. 117–128, 2012.

Bijl, P. K., Houben, A. J., Schouten, S., Bohaty, S. M., Sluijs, A., Reichart, G. J., ... and Brinkhuis, H.: Transient Middle Eocene atmospheric CO2 and temperature variations. Science, 330(6005), 819-821, https://doi.org/10.1126/science.1193654, 2010.

Bohaty, S. M., and Zachos, J. C.: Significant Southern Ocean warming event in the late middle Eocene. Geology, 31(11), 1017-1020, https://doi.org/10.1130/G19800.1, 2003.

Bohaty, S. M., Zachos, J. C., Florindo, F., and Delaney, M. L.: Coupled greenhouse warming and deep-sea acidification in the middle Eocene. Paleoceanography, 24(2), https://doi.org/10.1029/2008PA001676, 2009.

Bosboom, R. E., Abels, H. A., Hoorn, C., van den Berg, B. C., Guo, Z., and Dupont-Nivet, G.: Aridification in continental Asia after the middle Eocene climatic optimum (MECO). Earth and Planetary Science Letters, 389, 34-42, https://doi.org/10.1016/j.epsl.2013.12.014, 2014.

Bouilhol, P., Jagoutz, O., and Hanchar, J. M.: Dating the India–Eurasia collision through arc magmatic records, https://doi.org/10.1016/j.epsl.2013.01.023, 2013.

Boya, S.: El Sistema deltaico de la Arenisca de Sabiñánigo y la continentalización de la cuenca de Jaca. Ph.D. thesis. Universitat Autònoma de Barcelona, 2018.

Brasier, M. D., Shields, G., Kuleshov, V. N., and Zhegallo, E. A.: Integrated chemo-and biostratigraphic calibration of early animal evolution: Neoproterozoic–early Cambrian of southwest Mongolia. Geological Magazine, 133(4), 445-485, doi:10.1017/S0016756800007603, 1996.

Castelltort, S., Honegger, L., Adatte, T., Clark, J. D., Puigdefàbregas, C., Spangenberg, J. E., ... and Fildani, A.: Detecting eustatic and tectonic signals with carbon isotopes in deep-marine strata, Eocene Ainsa Basin, Spanish Pyrenees, Geology, 45(8), 707-710, https://doi.org/10.1130/G39068.1, 2003.

Chen, C., Guerit, L., Foreman, B. Z., Hassenruck-Gudipati, H. J., Adatte, T., Honegger, L., ... and Castelltort, S.: Estimating regional flood discharge during Palaeocene-Eocene global warming. Scientific reports, 8(1), 1-8, https://doi.org/10.1038/s41598-018-31076-3, 2018.

Coll, X., Gómez-Gras, D., Roigé, M., Teixell, A., Boya, S., and Mestres, N.: Heavy-mineral provenance signatures during the infill and uplift of a foreland basin: An example from the Jaca basin (southern Pyrenees, Spain). Journal of Sedimentary Research, 90 (12), 1747-1769, https://doi.org/10.2110/jsr.2020.084, 2020.

Cornaggia, F., Bernardini, S., Giorgioni, M., Silva, G. L., Nagy, A. I. M., and Jovane, L. ~~(2020).~~: Abyssal oceanic circulation and acidification during the Middle Eocene Climatic Optimum (MECO). Scientific reports, 10(1), 1-9, https://doi.org/10.1038/s41598-020-63525-3, 2020.

Cramwinckel, M. J., Van Der Ploeg, R., Bijl, P. K., Peterse, F., Bohaty, S. M., Röhl, U., and Sluijs,: A.Harmful algae and export production collapse in the equatorial Atlantic during the zenith of Middle Eocene Climatic Optimum warmth. Geology, 47 (3), 247-250, https://doi.org/10.1130/G45614.1, 2019.

Edgar, K. M., Wilson, P. A., Sexton, P. F., and Suganuma, Y.: No extreme bipolar glaciation during the main Eocene calcite compensation shift. Nature, 448 (7156), 908-911, https://doi.org/10.1038/nature06053, 2007.

Edgar, K. M., Wilson, P. A., Sexton, P. F., Gibbs, S. J., Roberts, A. P., and Norris, R. D.: New biostratigraphic, magnetostratigraphic and isotopic insights into the Middle Eocene Climatic Optimum in low latitudes. Palaeogeography, Palaeoclimatology, Palaeoecology, 297(3-4), 670-682, https://doi.org/10.1016/j.palaeo.2010.09.016, 2010.

Con formato: Inglés (Estados Unidos)

Con formato: Inglés (Estados Unidos)

Edgar, K. M., Bohaty, S. M., Coxall, H. K., Bown, P. R., Batenburg, S. J., Lear, C. H., and Pearson, P. N.: New composite bio-and isotope stratigraphies spanning the Middle Eocene Climatic Optimum at tropical ODP Site 865 in the Pacific Ocean. Journal of Micropalaeontology, 39(2), 117-138, https://doi.org/10.5194/jm-39-117-2020, 2020.

Espitalié, J., Deroo, G., and Marquis, F. : Rock-Eval pyrolysis and its applications. Revue De L'Institut Français Du Petrole, 40(5), 563-579, https://doi.org/10.2516/ogst:1985045, 1985.

Fio, K., Spangenberg, J. E., Vlahović, I., Sremac, J., Velić, I., and Mrinjek, E.: Stable isotope and trace element stratigraphy across the Permian–Triassic transition: A redefinition of the boundary in the Velebit Mountain, Croatia. Chemical Geology, 278(1-2), 38-57, https://doi.org/10.1016/j.chemgeo.2010.09.001, 2010.

Foreman, B. Z., Heller, P. L., and Clementz, M. T.: Fluvial response to abrupt global warming at the Palaeocene/Eocene boundary. Nature, 491(7422), 92-95, https://doi.org/10.1038/nature11513, 2012.

Foreman, B. Z., and Straub, K. M.: Autogenic geomorphic processes determine the resolution and fidelity of terrestrial paleoclimate records. Science advances, 3(9), https://doi.org/10.1126/sciadv.1700683, 2017.

Galazzo, F. B., Giusberti, L., Luciani, V., and Thomas, E.: Paleoenvironmental changes during the Middle Eocene Climatic Optimum (MECO) and its aftermath: The benthic foraminiferal record from the Alano section (NE Italy). Palaeogeography, Palaeoclimatology, Palaeoecology, 378, 22-35, https://doi.org/10.1016/j.palaeo.2013.03.018, 2013.

Galazzo, F.B., Thomas, E., Pagani, M., Warren, C., Luciani, V., and Giusberti, L.: The middle Eocene climatic optimum (MECO): A multiproxy record of paleoceanographic changes in the southeast Atlantic (ODP Site 1263, Walvis Ridge). Paleoceanography, 29(12), 1143-1161, https://doi.org/10.1002/2014PA002670, 2014.

Galy, V., France-Lanord, C., Beyssac, O. et al. Efficient organic carbon burial in the Bengal fan sustained by the Himalayan erosional system. Nature 450, 407–410, https://doi.org/10.1038/nature06273, 2007.

Garcés, M., López-Blanco, M., Valero, L., Beamud, E., Pueyo-Morer, E., and Rodríguez-Pinto, A.: Testing orbital forcing in the Eocene deltaic sequences of the South-Pyrenean Foreland Basins. EGU General Assembly Conference Abstracts (Vol. 16), 2014.

Giorgioni, M., Jovane, L., Rego, E.S., Rodelli, D., Frontalini, F., Coccioni, R., Catanzariti, R. and Özcan, E.: Carbon cycle instability and orbital forcing during the Middle Eocene Climatic Optimum. Sci Rep 9, 9357, https://doi.org/10.1038/s41598-019-45763-2, 2019.

Gradstein, F.M., Ogg, J.G., Schmitz, M. and Ogg, G.: The Geologic Time Scale 2012. Elsevier, Cambridge University Press, Cambridge, 2012.

Henehan, M. J., Edgar, K. M., Foster, G. L., Penman, D. E., Hull, P. M., Greenop, R., and Pearson, P. N.: Revisiting the Middle Eocene Climatic Optimum 'Carbon Cycle Conundrum' with new estimates of atmospheric pCO2 from boron isotopes. Paleoceanography and Paleoclimatology, https://doi.org/10.1029/2019PA003713 , 2020.

Homewood, P., Mauriaud, P., and Lafont, F.: Best practices in sequence stratigraphy: for explorationists and reservoir engineers (Vol. 25). Editions Technip, 2000.

Honegger, L., Adatte, T., Spangenberg, J. E., Caves Rugenstein, J. K., Poyatos, M., Puigdefàbregas, C., and Harlaux, M.: Alluvial record of an early Eocene hyperthermal, Castissent Formation, the Pyrenees, Spain. Climate of the Past, 16, 227-243, https://doi.org/10.5194/cp-16-227-2020, 2020.

Huyghe, D., Castelltort, S., Mouthereau, F., Serra-Kiel, J., Filleaudeau, P. Y., Emmanuel, L., ... and Renard, M.: Large scale facies change in the middle Eocene South-Pyrenean foreland basin: The role of tectonics and prelude to Cenozoic ice-ages. Sedimentary Geology, 253, 25-46, https://doi.org/10.1016/j.sedgeo.2012.01.004, 2012.

Jovane, L., Florindo, F., Coccioni, R., Dinarès-Turell, J., Marsili, A., Monechi, S., and Sprovieri, M.: The middle Eocene climatic optimum event in the Contessa Highway section, Umbrian Apennines, Italy. Geological Society of America Bulletin, 119(3-4), 413-427, https://doi.org/10.1130/B25917.1, 2007.

Klug, H. P., and Alexander, L. E.: X-ray diffraction procedures: for polycrystalline and amorphous materials (p. 992), 1974.

Kübler, B.: Dosage quantitatif des minéraux majeurs des roches sédimentaires par diffraction X: Neuchâtel, Suisse, Cahiers Institut Géologie, série ADX, Volume 1, 12 p, 1983.

Kübler, B.: Cristallinité de l'illite, méthodes normalisées de préparations, méthodes normalisées de mesures: Neuchâtel, Suisse, Cahiers Institut Géologie, série ADX, Volume 1, 13 p, 1987.

Kübler, B., and Jaboyedoff, M.: Illite crystallinity. Comptes Rendus de l'Académie des Sciences-Series IIA-Earth and Planetary Science, 331(2), 75-89, 2000.

Labaume, P., Meresse, F., Jolivet, M., and Teixell, A.: Exhumation sequence of the basement thrust units in the west-central Pyrenees. Constraints from apatite fission track analysis. Geogaceta, 60, 11-14, 2006.

Lafont, F.: Influences relatives de la subsidence et de l'eustatisme sur la localisation et la géométrie des réservoirs d'un système deltaïque. Exemple de l'Eocène du bassin de Jaca, Pyrénées espagnoles, Ph.D. thesis, Université Rennes, 1994.

Lagabrielle, Y., Labaume, P., and de Saint Blanquat, M.: Mantle exhumation, crustal denudation, and gravity tectonics during Cretaceous rifting in the Pyrenean realm (SW Europe): Insights from the geological setting of the lherzolite bodies. Tectonics, 29(4), https://doi.org/10.1029/2009TC002588, 2010.

Läuchli, C., Garcés, M., Beamud, E., Valero, L., Honegger, L., Adatte, T., and Castelltort, S.: Magnetostratigraphy and stable isotope stratigraphy of the middle-Eocene succession of the Ainsa basin (Spain): New age constraints and implications for sediment delivery to the deep waters. Marine and Petroleum Geology, 132, https://doi.org/10.1016/j.marpetgeo.2021.105182, 2021.

Lupker, M., France-Lanord, C., Lavé, J., Bouchez, J., Galy, V., Métivier, F., and Mugnier, J. L.: A Rouse-based method to integrate the chemical composition of river sediments: Application to the Ganga basin. Journal of Geophysical Research: Earth Surface, 116 (F4), https://doi.org/10.1029/2010JF001947, 2011.

Marshall, J. D.: Climatic and oceanographic isotopic signals from the carbonate rock record and their preservation. Geological magazine, 129(2), 143-160, doi:10.1017/S0016756800008244, 1992.

Con formato: Sin subrayado

Con formato: Sin subrayado

Con formato: Sin subrayado

Con formato: Sin subrayado

Millán, H., Aurell, M., and Meléndez, A.: Synchronous detachment folds and coeval sedimentation in the Prepyrenean External Sierras (Spain): a case study for a tectonic origin of sequences and systems tracts, Sedimentology, 41(5), 1001-1024, https://doi.org/10.1111/j.1365-3091.1994.tb01437.x, 1994.

Millán, H., Morer, E. P., Cardona, M. A., Aguado, A. L., Urcia, B. O., and Peña, B. M.: Actividad tectónica registrada en los depósitos terciarios del frente meridional del Pirineo central. Revista de la Sociedad Geológica de España, 13(2), 279-300, 2000.

Miller, K. G., Browning, J. V., Schmelz, W. J., Kopp, R. E., Mountain, G. S., and Wright, J. D.: Cenozoic sea-level and cryospheric evolution from deep-sea geochemical and continental margin records. Science advances, 6(20), https://doi.org/10.1126/sciadv.aaz1346, 2020.

Mochales, T., Barnolas, A., Pueyo, E. L., Serra-Kiel, J., Casas, A. M., Samsó, J. M., and Sanjuán, J.: Chronostratigraphy of the Boltaña anticline and the Ainsa Basin (southern Pyrenees). Bulletin, 124(7-8), 1229-1250, https://doi.org/10.1130/B30418.1, 2012.

Moebius, I., Friedrich, O., and Scher, H. D.: Changes in Southern Ocean bottom water environments associated with the Middle Eocene Climatic Optimum (MECO). Palaeogeography, palaeoclimatology, palaeoecology, 405, 16-27, https://doi.org/10.1016/j.palaeo.2014.04.004, 2014.

Moebius, I., Friedrich, O., Edgar, K. M., and Sexton, P. F.: Episodes of intensified biological productivity in the subtropical Atlantic Ocean during the termination of the Middle Eocene Climatic Optimum (MECO). Paleoceanography, 30(8), 1041-1058, https://doi.org/10.1002/2014PA002673, 2015.

Moore D.M., Reynolds R.C., X-ray diffraction and the identification and analysis of clay minerals, Oxford University Press, Oxford and New York, 1997.

Mulch, A., Chamberlain, C. P., Cosca, M. A., Teyssier, C., Methner, K., Hren, M. T., and Graham, S. A.: Rapid change in high-elevation precipitation patterns of western North America during the Middle Eocene Climatic Optimum (MECO). American Journal of Science, 315(4), 317-336, https://doi.org/10.2475/04.2015.02, 2015.

Muñoz, J.A.: Evolution of a continental collision belt: ECORS-Pyrenees crustal balanced cross-section. In: McClay, K.R. (eds) Thrust Tectonics. Springer, Dordrecht, https://doi.org/10.1007/978-94-011-3066-0_21, 1992.

Muñoz, J. A., McClay, K., and Poblet, J.: Synchronous extension and contraction in frontal thrust sheets of the Spanish Pyrenees. Geology, 22(10), 921-924, https://doi.org/10.1130/0091-7613(1994)022<0921:SEACIF>2.3.CO;2, 1994.

Muñoz, J. A., Beamud, E., Fernández, O., Arbués, P., Dinarès-Turell, J., and Poblet, J.: The Ainsa Fold and thrust oblique zone of the central Pyrenees: Kinematics of a curved contractional system from paleomagnetic and structural data. Tectonics, 32(5), 1142-1175, https://doi.org/10.1002/tect.20070, 2013.

Muñoz, J. A., Mencos, J., Roca, E., Carrera, N., Gratacós, O., Ferrer, O., and Fernández, O.: The structure of the South-Central-Pyrenean fold and thrust belt as constrained by subsurface data. Geologica Acta, 16(4), 439-460, 10.1344/GeologicaActa2018.16.4.7, 2018.

Con formato: Sin subrayado

Con formato: Sin subrayado

Con formato: Sin subrayado

Con formato: Sin subrayado

Con formato: Sin subrayado

Con formato: Sin subrayado

Mutti, E.: Distinctive thin-bedded turbidite facies and related depositional environments in the Eocene Hecho Group (South-central Pyrenees, Spain). Sedimentology, 24(1), 107-131, https://doi.org/10.1111/j.1365-3091.1977.tb00122.x, 1977.

Ogg, J. G., Ogg, G., and Gradstein, F. M.: A concise geologic time scale: 2016. Elsevier, Cambridge University Press, Cambridge, 2016.

Patterson, P.P. and Walter, L.M. Depletion of ^{13}C in seawater ΣCO_2 on modern carbonate platforms: Significance for the carbon isotopic record of carbonates. Geology, 22, 885–888, https://doi.org/10.1130/0091-7613(1994)022<0885:DOCISC>2.3.CO;2, 1994.

Pälike, H., Lyle, M. W., Nishi, H., Raffi, I., Ridgwell, A., Gamage, K., … and Baldauf, J.: A Cenozoic record of the equatorial Pacific carbonate compensation depth. Nature, 488(7413), 609-614, https://doi.org/10.1038/nature11360, 2012.

Pueyo, E. L., Millán, H., and Pocovı, A.: Rotation velocity of a thrust: a paleomagnetic study in the External Sierras (Southern Pyrenees). Sedimentary Geology, 146(1-2), 191-208, https://doi.org/10.1016/S0037-0738(01)00172-5, 2002.

Puigdefabregas. C.: La sedimentación molásica en la cuenca de Jaca. Pirineos. 104: I- 188, CSIC, Tesis Doctoral, 1975.

Puigdefàbregas, C., and Souquet, P.: Tecto-sedimentary cycles and depositional sequences of the Mesozoic and Tertiary from the Pyrenees, Tectonophysics, v. 129, p. 173–203, doi:10.1016/0040-1951(86)90251-9, https://doi.org/10.1016/0040-1951(86)90251-9, 1986.

Pujalte, V., Baceta, J. I., and Schmitz, B.: A massive input of coarse-grained siliciclastics in the Pyrenean Basin during the PETM: the missing ingredient in a coeval abrupt change in hydrological regime. Climate of the Past, 11 (12), https://doi.org/10.5194/cp-11-1653-2015 , 2015.

Remacha, E., and Fernández, L. P.: High-resolution correlation patterns in the turbidite systems of the Hecho Group (South-Central Pyrenees, Spain). Marine and Petroleum Geology, 20(6-8), 711-726, https://doi.org/10.1016/j.marpetgeo.2003.09.003, 2003.

Roigé, M., Gómez-Gras, D., Remacha, E., Daza, R., and Boya, S.: Tectonic control on sediment sources in the Jaca basin (Middle and Upper Eocene of the South-Central Pyrenees). Comptes Rendus Geoscience, 348(3-4), 236-245, https://doi.org/10.1016/j.crte.2015.10.005, 2016.

Roigé, M.: Procedència i evolució dels sistemes sedimentaris de la conca de Jaca (conca d'avantpaís Sudpirinenca): Interacció entre diverses àrees font en un context tectònic actiu. Universitat Autònoma de Barcelona. Tesis Doctoral, https://hdl.handle.net/10803/565902, 2018.

Roure, F., Choukroune, P., Berastegui, X., Munoz, J. A., Villien, A., Matheron, P., and Deramond, J.: ECORS deep seismic data and balanced cross sections: Geometric constraints on the evolution of the Pyrenees. Tectonics, 8(1), 41-50, https://doi.org/10.1029/TC008i001p00041, 1989.

Saltzman, M.R., and Thomas, E.: Carbon isotope stratigraphy, in Gradstein, F., et al., eds., The geologic time scale: Oxford, UK, Elsevier, p. 207–232, doi:10.1016/B978-0-444-59425-9.00011-1, 2012.

Schmitz, B., and Pujalte, V.: Abrupt increase in seasonal extreme precipitation at the Paleocene-Eocene boundary. Geology, 35(3), 215-218, https://doi.org/10.1130/G23261A.1, 2007.

Con formato: Sin subrayado

Con formato: Sin subrayado

Con formato: Superíndice

Con formato: Subíndice

Con formato: Sin subrayado

Con formato: Sin subrayado

Con formato: Español (España)

Con formato: Fuente: (Predeterminada) +Cuerpo (Times New Roman)

Con formato: Fuente: (Predeterminada) +Cuerpo (Times New Roman), Español (España)

Código de campo cambiado

Schrag, D. P., DePaolo, D. J., and Richter, F. M.: Reconstructing past sea surface temperatures: Correcting for diagenesis of bulk marine carbonate. Geochimica et Cosmochimica Acta, 59(11), https://doi.org/10.1016/0016-7037(95)00105-9, 1995.

Seguret, M.: Étude tectonique des nappes et séries décollées de la partie centrale du versant sud des Pyrénées. Pub. Ustela, Série Géologie structurale 2, 1-155, Montpellier, Ph.D. thesis, 1972.

Sluijs, A., Zeebe, R. E., Bijl, P. K., and Bohaty, S. M.: A middle Eocene carbon cycle conundrum. Nature Geoscience, 6(6), 429-434, https://doi.org/10.1038/ngeo1807, 2013.

Spangeberg, J.E., Herlec, U.: Hydrocarbon biomarkers in the Topla-Mezica zinc-lead deposits, northern Karavanke/Drau range, Slovenia: paleoenvironment at the site of ore formation, Economic Geology, 101 (5), 997-1021, https://doi.org/10.2113/gsecongeo.101.5.997, https://doi.org/10.2113/gsecongeo.101.5.997, 2006.

Spangeberg, J.E.: Bulk C, H, O, and fatty acid C stable isotope analyses for purity assessment of vegetable oils from the southern and northern hemispheres, Rapid Communications in Mass Spectrometry, 30 (23), 2447-2461, https://doi.org/10.1002/rcm.7734, 2016.

Spofforth, D. J. A., Agnini, C., Pälike, H., Rio, D., Fornaciari, E., Giusberti, L., ... and Muttoni, G.: Organic carbon burial following the middle Eocene climatic optimum in the central western Tethys. Paleoceanography, 25(3), https://doi.org/10.1029/2009PA001738, 2010.

Sternai, P., Caricchi, L., Pasquero, C., Garzanti, E., Hinsbergen, D. J. J., and Castelltort, S.: Magmatic Forcing of Cenozoic Climate?, Journal of Geophysics Research: Solid Earth, 125, 692–22, https://doi.org/10.1029/2018jb016460, 2020.

Swart, P. K.: The geochemistry of carbonate diagenesis: The past, present and future. Sedimentology, 62(5), https://doi.org/10.1111/sed.12205, 1995.

Sztrákos, K., and Castelltort, S.: La sédimentologie et les foraminifères bartoniens et priaboniens des coupes d'Arguis (Prépyrénées aragonaises, Espagne). Incidence sur la corrélation des biozones à la limite Bartonien/Priabonien. Revue de Micropaléontologie, 44(3), 233-247, https://doi.org/10.1016/S0035-1598(01)90185-0, 2001.

Teixell, A.: Crustal structure and orogenic material budget in the west central Pyrenees. Tectonics, 17(3), 395-406, https://doi.org/10.1029/98TC00561, 1998.

Teixell, A., Labaume, P., and Lagabrielle, Y.: The crustal evolution of the west-central Pyrenees revisited: inferences from a new kinematic scenario. Comptes Rendus Geoscience, 348(3-4), 257-267, https://doi.org/10.1016/j.crte.2015.10.010, 2016.

Teixell, A., Labaume, P., Ayarza, P., Espurt, N., de Saint Blanquat, M., and Lagabrielle, Y.: Crustal structure and evolution of the Pyrenean-Cantabrian belt: A review and new interpretations from recent concepts and data. Tectonophysics, 724, 146-170, https://doi.org/10.1016/j.tecto.2018.01.009, 2018.

Tribovillard, N., Algeo, T. J., Lyons, T., and Riboulleau, A.: Trace metals as paleoredox and paleoproductivity proxies: an update, Chemical geology, 232(1-2), 12-32, https://doi.org/10.1016/j.chemgeo.2006.02.012, 2006.

van der Weijden, C. H., Reichart, G. J. and van Os, B. J.: Sedimentary trace element records over the last 200 kyr from within and below the northern Arabian Sea oxygen minimum zone. Marine Geology, 231(1-4), 69-88, https://doi.org/10.1016/j.margeo.2006.05.013, 2006.

Con formato: Francés (Suiza)
Con formato: Francés (Suiza)
Con formato: Francés (Suiza)
Código de campo cambiado
Con formato: Francés (Suiza)
Con formato: Inglés (Estados Unidos)
Con formato: Inglés (Estados Unidos)
Con formato: Inglés (Estados Unidos)
Con formato: Inglés (Estados Unidos)
Con formato: Francés (Suiza)
Con formato: Francés (Suiza)
Con formato: Francés (Suiza)
Código de campo cambiado

Van Wagoner, J. C., Mitchum, R. M., Campion, K. M., and Rahmanian, V. D.: Siliciclastic sequence stratigraphy in well logs, cores, and outcrops: concepts for high-resolution correlation of time and facies, 1990.

Van Wagoner, J. C.: Sequence stratigraphy and marine to nonmarine facies architecture of foreland basin strata, Book Cliffs, Utah, USA: Reply. AAPG Bulletin, 82(8), 1607-1618, 1998.

Vergés, J., Fernàndez, M., and Martìnez, A.: The Pyrenean orogen: pre-, syn-, and post-collisional evolution. Journal of the Virtual Explorer, 8, 55-74, 10.3809/jvirtex.2002.00058, 2002.

Verité, J. : Enregistrement sédimentaire et climatique d'un hyperthermal en domaine continental : l'Optimum Climatique de l'Éocène Moyen dans le domaine Sud-Pyrénéen. Formation d'Escanilla, Espagne. Observatoire des Sciences de l'Univers de Rennes (France). Master Thesis, 2019.

Vinyoles, A., López-Blanco, M., Garcés, M., Arbués, P., Valero, L., Beamud, E., and Cabello, P.: 10 Myr evolution of sedimentation rates in a deep marine to non-marine foreland basin system: Tectonic and sedimentary controls (Eocene, Tremp–Jaca Basin, Southern Pyrenees, NE Spain). Basin Research, 33(1), 447-477, https://doi.org/10.1111/bre.12481, 2021.

Wendler, I.: A critical evaluation of carbon isotope stratigraphy and biostratigraphic implications for Late Cretaceous global correlation. Earth-Science Reviews, 126, 116-146, https://doi.org/10.1016/j.earscirev.2013.08.003, 2013.

Westerhold, T., and Röhl, U.: Orbital pacing of Eocene climate during the Middle Eocene Climate Optimum and the chron C19r event: Missing link found in the tropical western Atlantic. Geochemistry, Geophysics, Geosystems, 14 (11), 4811-4825, https://doi.org/10.1002/ggge.20293, 2013.

Zachos, J., Pagani, M., Sloan, L., Thomas, E., and Billups, K.: Trends, rhythms, and aberrations in global climate 65 Ma to present. science, 292(5517), 686-693, https://doi.org/10.1126/science.1059412, 2001.